

Proteomics unveil a central role for peroxisomes in butyrate assimilation of the heterotrophic Chlorophyte alga *Polytomella* sp.

1 **J. Lacroux¹, A. Atteia², S. Brugière³, Y. Couté³, O. Vallon⁴, J.-P. Steyer¹, R. van Lis^{1*}**

2 ¹INRAE, Univ Montpellier, LBE, 102 avenue des Etangs, F-11100, Narbonne, France

3 ²MARBEC, Univ Montpellier, CNRS, Ifremer, IRD, Sète, France

4 ³Univ Grenoble Alpes, CEA, INSERM, UMR BioSanté U1292, CNRS, CEA, FR2048, 38000
5 Grenoble, France

6 ⁴UMR7141 CNRS-Sorbonne Université, Institut de Biologie Physico-Chimique, Paris, France

7 ***Correspondence:**

8 Robert van Lis

9 robert.van-lis@inrae.fr

10 **Keywords: microalgae, volatile fatty acids, heterotrophy, quantitative proteomics, metabolic**
11 **pathways**

12 **Abstract**

13 Volatile fatty acids found in effluents of the dark fermentation of biowastes can be used for
14 mixotrophic growth of microalgae, improving productivity and reducing the cost of the feedstock.
15 Microalgae can use the acetate in the effluents very well, but butyrate is poorly assimilated and can
16 inhibit growth above 1 gC.L⁻¹. The non-photosynthetic chlorophyte alga *Polytomella* sp. SAG 198.80
17 was found to be able to assimilate butyrate fast. To decipher the metabolic pathways implicated in
18 butyrate assimilation, quantitative proteomics study was developed comparing *Polytomella* sp. cells
19 grown on acetate and butyrate at 1 gC.L⁻¹. After statistical analysis, a total of 1772 proteins were
20 retained, of which 119 proteins were found to be overaccumulated on butyrate vs. only 46 on acetate,
21 indicating that butyrate assimilation necessitates additional metabolic steps. The data show that
22 butyrate assimilation occurs in the peroxisome via the β -oxidation pathway to produce acetyl-CoA
23 and further tri/dicarboxylic acids in the glyoxylate cycle. Concomitantly, reactive oxygen species
24 defense enzymes as well as the branched amino acid degradation pathway were strongly induced.
25 Although no clear dedicated butyrate transport mechanism could be inferred, several membrane
26 transporters induced on butyrate are identified as potential candidates. Metabolic responses
27 correspond globally to the increased needs for central cofactors NAD, ATP and CoA, especially in
28 the peroxisome and the cytosol.

29 **1 Introduction**

30 Mixotrophic growth combines the reduction of CO₂ via photosynthesis with the oxidation of organic
31 carbon and is found in a wide range of phototrophic microorganisms such as cyanobacteria and
32 microalgae (Perez-Garcia and Bashan, 2015). This trophic mode is generally the most efficient in terms
33 of biomass productivity (Zhan et al., 2017). Some photosynthetic microalgae also have heterotrophic
34 capacities, i.e. they can grow in the absence of light on reduced carbon sources (Round, 1980).
35 Although glucose can yield very high biomass productivities (Perez-Garcia et al., 2011), it is an

36 expensive substrate that is not economical for many microalgal biorefinery applications with lower
37 added value such as biofuels, green chemistry platform molecules, aquaculture and biofertilizer (Acién
38 Fernández et al., 2019). It has been proposed to use organic acids produced by the fermentation of
39 biowaste material as feedstock to lower the cost (Delrue et al., 2016; Turon et al., 2016; Chalima et al.,
40 2017; Karnaouri et al., 2020). Dark fermentation (DF) of organic matter by microbial consortia is a
41 sustainable method for H₂ production that compares favorably to other process in terms of CO₂
42 footprint (Dincer and Acar, 2015; Moscoviz et al., 2018). In this context it is warranted to intensify
43 research on downstream coupled processes such as mixotrophic cultivation of microalgae on DF
44 effluents (DFE). Depending on the conditions, DFEs contain different ratios of volatile fatty acids
45 (VFA) alongside some lactate and ethanol. In general, mostly acetate and butyrate are present, in a
46 molar ratio of 0.66 on average (Turon et al., 2016; Moscoviz et al., 2018).

47 While microalgae that use glucose can usually also use acetate, many algae can grow on acetate but
48 not on glucose, e.g. *Chlamydomonas reinhardtii* (Harris, 1989). Capacities for the use of other
49 substrates such as lactate, ethanol and butyrate are less common and vary widely, even within the same
50 species e.g. *Euglena gracilis var bacillaris* or *urophora* (Neilson and Lewin, 1974; Hosotani et al.,
51 1988). By far the most abundant VFA in DFEs is butyrate, but it is toxic for many bacteria and is
52 known to be poorly used by microalgae (Turon et al., 2015; Lacroux et al., 2020, 2021). A generalized
53 toxicity effect of VFAs is observed as the extracellular pH approaches the pK_a value because cells are
54 permeable to the protonated form, resulting in deleterious effect on the cell metabolism and integrity
55 (Lacroux et al., 2020). The toxicity threshold for butyrate (as butyric acid) is 5-fold lower than for
56 acetic acid in some species, explaining why it is a poor carbon source. Algal growth on butyrate will
57 thus require more care in adapting the pH and concentration to remain below the observed species-
58 specific toxicity threshold. However, this will be inadequate to reach growth rates similar to those on
59 acetate. It is therefore crucial that butyrate metabolism be studied in detail in order to remove metabolic
60 bottlenecks in its assimilation.

61 Butyrate assimilation is well studied in microorganisms such as the sulfate reducer *Desulfosarcina*
62 *cetonica* (Janssen and Schink, 1995), the non-sulfur purple bacterium *Rhodospirillum rubrum* (De
63 Meur et al., 2020), yeasts i.e. *Candida ingens* (Garrison et al., 1985) or *Yarrowia lipolytica* (Llamas et
64 al., 2020) and also in human colonocytes, for which bacteria-produced butyrate is the primary energy
65 source (Roediger, 1982; Fleming et al., 1991). Colonocytes import butyrate via the monocarboxylate
66 transporter (MCT), a 45-kDa plasma membrane protein with 12 transmembrane segments that
67 symports H⁺ with the butyrate anion (Cuff et al., 2005). Butyrate is subsequently imported into the
68 mitochondrial matrix where it undergoes β-oxidation to acetyl-CoA, which in turn enters the TCA
69 cycle resulting in the production of NADH. The first step of β-oxidation is its activation into butyryl-
70 CoA via an ATP-dependent butyryl-CoA synthetase, followed by the conversion into crotonyl-CoA
71 by butyryl-CoA dehydrogenase, into hydroxy-isobutyryl-CoA by enoyl-CoA hydratase, then into
72 acetoacetyl-CoA by hydroxybutyryl-CoA dehydrogenase and finally into acetyl-CoA via acetoacetyl-
73 CoA thiolase (De Preter et al., 2012). A different assimilation metabolism was uncovered by a
74 proteomic approach in the non-sulfur purple bacterium *R. rubrum* (De Meur et al., 2020), where acetyl-
75 CoA is used to activate butyrate via butyryl-CoA:acetate CoA transferase under photoheterotrophic
76 conditions. Homologs of most enzymes potentially involved in butyrate assimilation as found in human
77 colonocytes have been identified in *C. reinhardtii*, the best studied algal species (Li-Beisson et al.,
78 2019). However, nothing is known about the enzyme(s) that may be involved in formation of butyryl-
79 CoA in algae, in particular their subcellular localization. The case of acetyl-CoA is better studied. In
80 the model alga *C. reinhardtii*, acetyl-CoA is formed from acetate by acetyl-CoA synthase, purportedly
81 in peroxisomes, and further utilized in the glyoxylate cycle to form products such as malate, citrate and
82 succinate that can be further exported to other cell compartments (Lauersen et al., 2016). The import
83 of butyrate into microalgal cells and the associated metabolic responses and their intracellular
84 localization remain to be studied.

85 The heterotrophic chlorophyte *Polytomella* sp. SAG 198.80 is to our knowledge the alga for which
86 the fastest butyrate assimilation has been described (Wise, 1955, 1959), and more recently by the
87 authors of this work (Lacroux et al. 2022). The fact that *Polytomella* has lost photosynthetic activity
88 allows focusing on the assimilation pathways, avoiding interactions with photosynthetic metabolism
89 that complicate analysis (van Lis and Atteia, 2004; Johnson and Alric, 2013). In this study, a
90 quantitative proteomics approach is used to decipher the metabolic pathways specifically involved in
91 the assimilation of butyrate by *Polytomella*, based on the comparison to acetate as reference
92 metabolism as this is the simplest entry of organic carbon into central carbon metabolism.

93 2 Material and methods

94 2.1 Strain and culture conditions

95 *Polytomella* sp. SAG 198.80 was obtained from the SAG culture collection (Goettingen, Germany).
96 It was grown on synthetic media referred to as HAP (acetate) or HBP (butyrate), based on Tris-
97 Acetate-Phosphate (TAP) medium used for the green alga *C. reinhardtii* (Harris, 1989), in which the
98 Tris buffer is replaced by HEPES 0.1 M, at pH 7. Beijerincks solution (40X) was used at 25 mL.L⁻¹
99 leading to an ammonium (NH₄⁺) concentration of 7.5 mM, 0.6 mM of MgSO₄ and 0.3 mM of CaCl₂.
100 To adjust nutrients to the Redfield C:N:P ratio of 106:16:1, corresponding to 83.3:12.6:0.8 mM for 1
101 g carbon per liter (1.0 gC.L⁻¹), the proper amount of 1 M NH₄Cl (5 mL) and 1 M K₂HPO₄ (0.8 mL)
102 stock solutions were added. Hutner's trace elements were used at 1 mL.L⁻¹ (Hutner, 1972). As carbon
103 source, acetate or butyrate were added as sodium salts at 1.0 gC.L⁻¹ (41.7 mM acetate, 20.8 mM
104 butyrate) and pH medium was adjusted to 7.0 (HCl) prior to sterilization at 121°C for 20 min. After
105 cooling, 100 µL.L⁻¹ was added of a stock of vitamin B1 (50 mM), biotin (1 mM) and cyanocobalamin
106 (1 mM), sterilized over a 0.2 µm filter. Precultures were maintained on HAP medium containing 20
107 mM HEPES and were used to inoculate HAP and HBP media to initial optical density at 750 nm
108 (OD₇₅₀) = 0.05. The inoculum was prepared by collecting preculture cells in their exponential phase
109 via centrifugation at 2500 g for 10 min, and resuspending them in Phosphate Buffered Saline to a
110 final OD₇₅₀ = 5. Cultures were done in 500mL Erlenmeyer flasks filled with 200 mL medium under
111 dim light at 25°C and without agitation.

112 2.2 Biomass and VFA measurement

113 Biomass growth was followed by measuring optical density at 750 nm (OD₇₅₀), using a Helios
114 Epsilon spectrophotometer. OD₇₅₀ was measured by placing 1 mL of liquid culture in a cuvette and
115 comparing to distilled water. The sample was diluted when necessary so that OD₇₅₀ < 0.6. Biomass
116 production was expressed in g.L⁻¹ dry weight (DW) deduced from OD₇₅₀ determination. To
117 calculate the biomass DW from OD₇₅₀ values, a correlated factor was used, determined to be 1.0774
118 (R² = 0.977). This correlation factor was obtained from a calibration curve gathering 70 data points
119 collected during separated experiments, at various growth stages (stationary phase excluded) and
120 growth conditions (HAP or HBP medium). To determine biomass DW during these experiments,
121 between 5 and 25 mL (depending on growth stage) biomass was centrifuged (3000 rpm, 10 min).
122 Supernatant was discarded, and pellet rinsed with one volume of phosphate buffer saline. Biomass
123 was centrifuged again, supernatant discarded and pellet resuspended in 10 mL distilled water. The
124 biomass was transferred in a pre-dried and pre-weighed aluminium crucible and dried overnight at
125 105°C.

126 For VFA measurements, samples from fresh cultures were immediately centrifuged, the supernatant
127 filtered over 0.2 µm cut-off filters and frozen at -25°C until analyzed. The VFA concentrations were
128 determined by gas chromatography. A 500 µL aliquot of supernatant was mixed with 500 µL of

129 internal standard solution (ethyl-2-butyric acid, 1 g·L⁻¹). The GC system consisted in a Perkin Clarus
130 580 model equipped with capillary column Elite-FFAP crossbond®carb Wax® (15 m) maintained at
131 200 °C and with N₂ as the gas vector (flow rate of 6 mL·min⁻¹) with a flame ionization detector (FID)
132 maintained at 280 °C (PerkinElmer, USA)

133 **2.3 Analysis of total lipids and sugars**

134 Samples from fresh cultures were immediately centrifuged, the supernatants were discarded and the
135 pellets stored at -25°C until used. Prior to analysis, the pellet was thawed, resuspended in 100µl
136 distilled water and added to 10 mL glass tubes for either lipid or sugar measurement. Total lipid
137 concentrations in the algal samples were determined by the phosphovanillin method (Mishra et al.,
138 2014). Phosphovanillin reagent was freshly prepared by first dissolving 0.6 g vanillin in 10 ml
139 ethanol, and then adding 90 ml deionized water and 400 ml of H₃PO₄ (85%). The resulting reagent
140 was stored in the dark. First, 2 mL H₂SO₄ (98%) were added in the tubes containing microalgae cells.
141 The tubes were heated 10 min at 100° C and cooled on ice. The reaction was initiated by addition of
142 5 mL phosphovanillin reagent prior incubation for 15 min at 37° C. Tubes were periodically shaken
143 by inversion. After cooling, optical density of suspensions was measured at 530 nm with an
144 Aqualytic® spectrometer and compared to distilled water. Calibration curves were obtained using
145 canola oil.

146 Total sugars were measured by the anthrone method (Yemm and Willis, 1954). Anthrone reagent was
147 prepared by dissolving 200 mg of anthrone in 100 mL of H₂SO₄ (98%). Two mL of anthrone reagent
148 were added in the tubes containing microalgae. Tubes were cooled down on ice and then incubated at
149 100° C for 10 min. After cooling, absorbance was measured at 625 nm with an Aqualytic®
150 spectrometer and compared to distilled water. Calibration curves were obtained using glucose
151 solution.

152 **2.4 Calculation of specific rates and product yield in growing cultures**

153 The biomass productivity P_x (g_{dw}·L⁻¹·d⁻¹) and the specific growth rate μ_x (d⁻¹) were calculated
154 according to equations (1) and (2):

$$155 \quad P_x = \frac{X_f - X_0}{t_f - t_0} \quad (1)$$

$$156 \quad \mu_x = \frac{\ln(X_f/X_0)}{(t_f - t_0)} \quad (2)$$

157 where X_f and X_0 are the biomass concentrations at t=final (h) and at t=0h.

161 The biomass yield Y (g_{dw}·g_{sub}⁻¹) was estimated according to equation (3):

$$162 \quad Y_s = \frac{S_0 - S_f}{t_f - t_0} \quad (3)$$

163 Where S_f and S_0 are substrate concentrations (g·L⁻¹) at t=final (h) and at t=0h.

166 Statistical analysis was performed using GraphPad Prism V 8.0.2.

169 **2.5 Mass spectrometry-based proteomic analyses**

170 The total proteome of *Polytomella* sp. grown either on acetate or butyrate (three biological replicates
171 per condition) were stacked in the top of a 12% SDS-PAGE resolving gel before in-gel digestion
172 using modified trypsin (sequencing grade, Promega), as previously described (Casabona et al., 2013).
173 The resulting peptides were analyzed by online nanoliquid chromatography coupled to MS/MS
174 (Ultimate 3000 RSLCnano and Q-Exactive HF, Thermo Fisher Scientific) using a 80 min gradient.
175 For this purpose, the peptides were sampled on a precolumn (300 μ m x 5 mm PepMap C18, Thermo
176 Scientific) and separated in a 75 μ m x 250 mm C18 column (Reprosil-Pur 120 C18-AQ, 1.9 μ m, Dr.
177 Maisch). The MS and MS/MS data were acquired by Xcalibur (Thermo Fisher Scientific).
178 Peptides and proteins were identified by Mascot (version 2.6.0, Matrix Science) through concomitant
179 searches against a homemade *Polytomella* sp. database, a homemade classical database containing
180 the sequences of classical contaminant proteins found in proteomic analyses (human keratins, trypsin,
181 etc.), and the corresponding reversed databases. Trypsin/P was chosen as the enzyme and two missed
182 cleavages were allowed. Precursor and fragment mass error tolerances were set at respectively at 10
183 ppm and 25 mmu. Peptide modifications allowed during the search were: Carbamidomethyl (C,
184 fixed), Acetyl (Protein N-term, variable) and Oxidation (M, variable). The Proline software
185 (Bouyssié et al., 2020) was used for the compilation, grouping, and filtering of the results
186 (conservation of rank 1 peptides, peptide length ≥ 7 amino acids, peptide-spectrum-match score ≥ 25 ,
187 allowing to reach a false discovery rate of peptide-spectrum-match identifications $< 1\%$ as calculated
188 on peptide-spectrum-match scores by employing the reverse database strategy, and minimum of one
189 specific peptide per identified protein group). Proline was then used to perform MS1 quantification
190 of the identified protein groups based on specific peptides.
191 Statistical analysis was performed using the ProStaR software (Wieczorek et al., 2017).
192 The mass spectrometry proteomics data have been deposited to the ProteomeXchange Consortium
193 via the PRIDE (Perez-Riverol et al., 2022) partner repository with the dataset identifier PXD035155.
194 Proteins identified in the contaminant database, and proteins detected in less than three replicates of
195 one condition were removed. After log₂ transformation, abundance values were normalized by the
196 vsn method before missing value imputation (slsa algorithm for partially observed values in the
197 condition and DetQuantile algorithm for totally absent values in the condition). Statistical testing was
198 conducted with limma, whereby differentially expressed (DE) proteins were sorted out using a
199 log₂(fold change) cut-off of 0.6 and a p-value cut-off of 0.004, allowing to reach a false discovery
200 rate $< 1\%$ according to the Benjamini-Hochberg method.
201 Intensity-based absolute quantification (iBAQ, Schwanhäusser et al., 2011) values were calculated
202 from MS intensities of specific peptides. For each sample, the iBAQ value of each protein was
203 normalized by the summed iBAQ value of all proteins, before summing the values of the three
204 replicates to generate the final iBAQ value of each condition.

205 **2.6 Bioinformatic analyses**

206 The assembly and structural annotation of the genome sequence of *Polytomella* sp. was described
207 previously (van Lis et al., 2021). The predicted proteins (genome to be released at a later date) were
208 used for the construction of the database for proteomics analysis. The functional annotation of the
209 proteins that were identified by proteomics (1772 sequences) and further attribution of metabolic
210 categories was done using Mercator4 V3.0 (<https://plabipd.de/portal/mercator4>), and used to project
211 the fold change data onto a metabolic overview SVG image file, using the MapMan program
212 (<https://plabipd.de/portal/mapman>) (Schwacke et al., 2019) used as stand-alone desktop application
213 and Inkscape (<https://inkscape.org/release/inkscape-1.2.1/>) to modify the image file.
214 Final metabolic pathway reconstructions were based on metabolic maps made in KEGG mapper
215 using KEGG and EC codes from BlastKOALA and KofamKOALA (HMM) homology searches at
216 KEGG (<https://www.genome.jp/kegg/>) and by using EggNOG (Huerta-Cepas et al., 2019). These

217 programs were also used to confirm and adjust annotations from Mercator where necessary, as well
218 as manual BLAST searches using the UniProt database (<https://www.uniprot.org>) and the *C.*
219 *reinhardtii* genome at Phytozome 13 (<https://phytozome-next.jgi.doe.gov>). OmicsBox 1.3.11
220 (<https://www.biobam.com/omicsbox>) genome blast was used with the genomes of *Chlamydomonas*
221 *reinhardtii* (Uniprot UP000006906) and *Chlorella sorokiniana* (Uniprot UP000239899) to obtain
222 equivalent enzyme identities in these two model microalgae. For subcellular localization predictions,
223 DeepLoc (Almagro Armenteros et al., 2017) and PredAlgo (Tardif et al., 2012) were used with the
224 limitation that the latter does not predict peroxisomal targeting. Therefore further searches for
225 potential peroxisome targeting signals in *Polytomella* protein sequences were done with the PTS1
226 predictor (<https://mendel.imp.ac.at/pts1/>) (Neuberger et al., 2003) or manually based on (Gonzalez et
227 al., 2011).

228 3 Results & Discussion

229 3.1 *Polytomella* sp. is a suitable model for the study of butyrate metabolism

230 At the basis of this work is the choice of *Polytomella* sp. as model algal species for the study of butyrate
231 metabolism. The genus *Polytomella* belongs to the Reinhardtinia clade of Volvocine algae (Craig et
232 al., 2021) and has diverged from a *Chlamydomonas*-like ancestor after having lost photosynthesis along
233 with the chloroplast genome (Smith and Lee, 2014). *Chlamydomonas reinhardtii* only grows
234 efficiently on acetate (Harris, 2001), so the highly versatile heterotrophic metabolism allowing
235 *Polytomella* to grow on a multitude of alcohols and organic acids including butyrate (Wise, 1955, 1959;
236 Round, 1980; de la Cruz and Gittleson, 1981) may have been partly acquired after the divergence. The
237 availability of an annotated genome sequence of *Polytomella* sp. (van Lis et al., 2021) allowed a global
238 proteomics approach to decipher its metabolic pathways involved in the assimilation of butyrate. Cells
239 grown on either acetate or butyrate, at a fixed C concentration of 1.0 gC.L⁻¹ (Fig. 1) showed similar
240 growth rates of 2.37 d⁻¹ ± 0.07 and 2.23 d⁻¹ ± 0.08, respectively (three biological triplicates). Both
241 carbon sources were completely consumed before 1.5 days, leading to a maximum biomass yield of
242 1.07 g_x.L⁻¹ (x=dry weight biomass) in both conditions (Fig 1C). After organic carbon exhaustion,
243 biomass declined due to cell death in both conditions and cysts formation was observed (not shown).
244 Biomass growth was accompanied by sugar accumulation, with about 15% less sugar on butyrate than
245 on acetate (Fig 1D). In the related species *P. agilis*, the accumulated sugar was found to be essentially
246 starch (Sheeler et al., 1968). Lipid accumulation is low in both cells, with a maximum of 73.3 ± 3.6
247 mg.L⁻¹ (biomass content ~5%) on acetate and 55.6 ± 3.1 mg.L⁻¹ on butyrate.

248 For several *Chlorella* strains it was reported that butyrate assimilation, when it occurred, was slower
249 than acetate assimilation (Liu et al., 2013; Fei et al., 2015). Heterotrophic (dark) growth rates of
250 *Chlorella sorokiniana* are 2.23 d⁻¹ on acetate and 0.16 d⁻¹ on butyrate (Turon et al., 2015). The ability
251 of *Polytomella* sp. to grow on butyrate with a growth rate of 2.2 d⁻¹, similar to that on acetate (Fig 1C),
252 is thus remarkable.

253 Green microalgae tend to accumulate proteins during exponential growth and only start synthesizing
254 storage compounds (starch, lipids) when growth conditions become suboptimal, e.g. when a micro- or
255 macro-element such as nitrogen is limiting (Dincer and Acar, 2015). Since this fact usually implies
256 that high biomass productivity is accompanied by low starch or lipid accumulation, continuous
257 cultivation is less relevant (Adams et al., 2013). Accumulation of high levels of starch during the
258 exponential growth phase is thus another distinctive and interesting trait of *Polytomella* sp..

259 3.2 Comparing global proteomes

260 Cultures of *Polytomella* sp. growing on acetate and butyrate were sampled during the exponential phase
261 (arrows in Fig. 1). Total cell proteins were first analyzed on SDS-PAGE stained with Coomassie Blue

262 G250. From the comparison of the protein profiles (Fig. 2A) it is inferred that butyrate elicits major
263 changes in protein levels, and a clear upregulation of 3 proteins of 28, 38 and 60 kDa can be observed
264 (indicated by asterisks, Fig 2A). To study more in detail the proteomic responses to butyrate, total
265 proteins from acetate and butyrate grown cells were subjected to mass spectrometry (MS)-based label-
266 free quantitative proteomic analysis. A volcano plot depicts the acetate vs butyrate fold change (FC, a
267 direct measure of the relative protein abundance between both conditions) and the associated statistical
268 significance (limma p-value) for each protein (Fig. 2B). The $\log_2(\text{FC})$ values varied between 4 and -
269 10, corresponding to an FC of 16 and 0.001, where the latter value indicates a 1000-fold upregulation
270 on butyrate. A total of 1772 proteins were retained after statistical analysis, of which 119 were found
271 to be significantly more abundant on butyrate compared to only 46 on acetate, and usually with a lower
272 FC. This shows that growth on butyrate is accompanied by overaccumulation of a larger set of proteins
273 than on acetate, which may indicate that butyrate needs more metabolic steps to enter central carbon
274 metabolism than acetate.
275

276 3.3 Proteomic responses per metabolic category

277 The 1772 proteins identified by MS-based proteomics were grouped into 27 metabolic categories using
278 the Mercator program, which was conceived for plant sequences but can also be used for microalgae
279 (May et al., 2008; Davidi et al., 2014), including *Polytomella* sp (Fuentes-Ramírez et al., 2021). Several
280 other databases were used to confirm identities in case of doubt especially for the entries listed in Table
281 I, as described in the Material and Methods section. Any redundant entries in the Mercator results were
282 removed and retained in only one metabolic category. Of the 1772 statistically relevant proteins, 217
283 could not be annotated (12.2%) and 411 were annotated but could not be assigned to any Mercator
284 category (23.2%) (Fig 3A). These percentages are similar or significantly lower than found in whole
285 cell proteomic studies of other microalgae such as *C. reinhardtii* or *Dunaliella bardawil* (May et al.,
286 2008; Davidi et al., 2014). A number of proteins that were not readily categorized but to which an EC
287 number could be assigned, were included in the category 'Enzyme classification'. The "protein
288 biosynthesis" category is the metabolic category most represented with 209 proteins (11.8% of total
289 proteins), followed by "protein homeostasis" (99 proteins; 5.6%) and "lipid metabolism" (84 proteins;
290 4.7%) (Fig. 3A). In addition, we calculated the cumulated iBAQ values to yield the total protein
291 abundance per Mapman category in both conditions (Fig. 3B). The iBAQ value of a protein reflects its
292 intra-sample abundance, and this calculation thus tries to estimate the impact of a condition on the
293 accumulation of proteins related to a certain pathway. Among identified proteins, those in the
294 categories "protein biosynthesis" and "cellular respiration" contribute most to the cumulative iBAQ
295 value. Two major differences are seen between the two conditions. For acetate there is a more
296 pronounced accumulation of proteins involved in protein biosynthesis (29% compared to 19.2% for
297 butyrate), whereas for butyrate an enrichment is observed for proteins involved in lipid metabolism
298 (11.8% vs 4.5% for acetate). It is noted that the two unassigned categories (annotated or not annotated)
299 each contribute proportionally much less to the total iBAQ than to the number proteins, reflecting the
300 fact that high abundance proteins are more likely to be attributed to a specific function.
301 Focussing on proteins differentially-expressed (DE) between the acetate and butyrate conditions, the
302 above global trend is confirmed but a more detailed picture emerges (Fig. 4). Relative to acetate, more
303 proteins are overaccumulated on butyrate in the categories related to primary metabolism *i.e.* cellular
304 respiration (4), carbohydrate metabolism (17), amino acid metabolism (10) and lipid metabolism (25),
305 as well as the categories redox homeostasis (9), solute transport (10) and coenzyme metabolism (5). In
306 contrast, acetate grown cells overaccumulate more proteins involved in homeostasis (6), biosynthesis
307 (13) and protein translocation (2) as well as in RNA processing (4), processes that can be considered
308 as necessary for general cellular maintenance. Comparing the proportion of FC proteins in each

309 category to the proportion in these categories of the 1772 identified proteins using the Exact Fisher's
310 test, a significant enrichment in butyrate was obtained for the categories carbohydrate- and lipid
311 metabolism, redox homeostasis and solute transport. For the acetate condition, the protein biosynthesis
312 and protein homeostasis were found enriched. Overall, it is clear that the butyrate utilization mobilizes
313 a higher number of proteins, suggesting a more profound metabolic response compared to acetate.
314

315 **3.4 Metabolic pathways involved in butyrate response**

316 To obtain a global metabolic representation of *Polytomella* sp., MapMan was used to project the FC
317 values of individual proteins onto the different metabolic pathways. In section 3.5 these pathways will
318 be discussed in detail. In the category lipid metabolism, the highest FC values are for enzymes of fatty
319 acid synthesis, fatty acid degradation and the glyoxylate cycle (Fig. 5). The enzymes of the latter two
320 functional groups are predicted to localize mostly to the peroxisomes, based on peroxisomal targeting
321 prediction via software algorithms, manual analysis of the presence of peroxisomal targeting sequences
322 PST1 and PST2, and/or the relatedness to peroxisomal enzymes in the green alga *C. reinhardtii* (Table
323 I; see also suppl. Table I). Peroxisomes, organelles primarily dedicated to peroxide detoxification, seem
324 to play a major role in butyrate assimilation in *Polytomella*. Butyrate being a fatty acid, the MapMan
325 category "fatty acid degradation" is expected, and corresponds to what is described for other organisms
326 (De Preter et al., 2012; De Meur et al., 2020). The glyoxylate cycle upregulation is in line with the fact
327 that butyrate degradation leads to the production of 2 molecules of acetyl-CoA, which together with
328 glyoxylate is the central entry point into the cycle. Fatty acid synthesis is also upregulated and is related
329 in part to the activation with Coenzyme A, and seems to indicate cellular shift in the production sites
330 and levels of acetyl-CoA (Pietrocola et al., 2015). Fatty-acid synthesis intermediates may for example
331 be needed for the production of cofactors such as biotin and lipoic acid (Alban et al., 2000). Indeed,
332 several enzymes involved in cofactors synthesis were found to be strongly upregulated as well. In
333 addition, several enzymes (such as catalase) involved in antioxidant defense were strongly upregulated
334 (Fig. 5), which can be directly or indirectly a consequence of the degradation of butyrate, notably by
335 the formation of H₂O₂ at the site of the acyl-CoA oxidase (ACX) enzyme (Kato et al., 2021) but also
336 due to the fact that butyrate is 25% more reduced compared to acetate, leading to an increased
337 generation of reducing equivalents such as NADH.

338 The amino acid metabolic pathway most affected by the C-source is the formation and subsequent
339 degradation of branched chain amino acids (BCAAs). It appears to take place largely in the peroxisome
340 based on the subcellular targeting predictions of the corresponding proteins, unlike in its close relative
341 *C. reinhardtii* where it occurs in the mitochondria (Liang et al., 2019). It is noted that some of these
342 enzymes are partitioned by MapMan into the lipid metabolism category. Carbohydrate metabolism,
343 notably starch degradation, is upregulated on butyrate, reflected in the lower starch content in butyrate
344 grown cells (Fig. 1D), which suggests an increased mobilization of glucose into pyruvate for
345 downstream metabolic pathways. Finally, several peroxisomal and mitochondrial-type solute
346 transporters are clearly induced on butyrate, which indicates increased exchange of a variety of
347 metabolites between these compartments.
348

349 **3.5 Reconstruction of the butyrate metabolic network**

350 A list of those proteins that exhibit the most pronounced fold change sorted according to the Mercator
351 categories is presented in Table I, alongside the most relevant data pertaining to protein databases and
352 proteomic parameters. Protein identities were obtained by homology searches using Mercator and other
353 programs for further validation (see material and methods), and their functional characteristics and

354 their known or predicted intracellular localization were used to reconstruct the most important
355 metabolic pathways in *Polytomella* sp. cells growing on butyrate relative to acetate. The most
356 pronounced enrichment of enzymes involved in butyrate assimilation is found in the peroxisomes,
357 small spherical organelles (0.2-1.5µm) that lack DNA and are surrounded by a single membrane that
358 derives from the endoplasmic reticulum (Hu et al., 2012). Originally described as organelles that harbor
359 oxidases that produce H₂O₂ and catalase for its detoxification (De Duve and Baudhuin, 1966), they are
360 known to compartmentalize a large diversity of functions among which fatty acid β-oxidation
361 (Gabaldón, 2010). In *Polytomella caeca*, small organelles distinct from mitochondria were identified
362 that contained catalase activity (Gerhardt, 1971). Although previously typical peroxisomes could not
363 be identified in *C. reinhardtii* (Silverberg, 1975), recently the β-oxidation enzyme acyl-CoA oxidase
364 as well as catalase were identified in peroxisomes (Kong et al., 2017; Kato et al., 2021). Also, the
365 enzymes of the glyoxylate cycle were shown in *C. reinhardtii* to localize to the peroxisome (or
366 glyoxysome) (Lauersen et al., 2016). The proposed butyrate metabolic network is depicted in Fig. 6
367 and 7. Its operation depends not only on the presence of the appropriate enzymes, but also on their
368 intracellular localization. Unfortunately, intracellular locales remain uncertain for some enzymes, due
369 to lack of experimental evidence, possible N-terminal truncation of the gene models and ambiguous or
370 obviously erroneous results from the prediction algorithms, which have not been trained specifically
371 for *Polytomella*. Still, for most of the highly butyrate-induced proteins, reasonable deductions could be
372 made that permit drawing a coherent picture of the intracellular location of the involved metabolic
373 pathways (Table I).
374

375 **3.5.1 Peroxisomal butyrate assimilation pathway**

376 Once butyrate is taken up by the cell it must be activated to butyryl-CoA before it can enter the β-
377 oxidation pathway in the peroxisome (Fig. 6). Candidates for this function were sought among the
378 proteins most highly induced by butyrate. The highest induction level (FC 0.002; see Table I for
379 Log₂FC values) was found for g1889, which harbors at its C-terminus a typical PTS1 signal
380 (Neuberger et al, 2003). It was annotated by Mercator as long-chain acyl-CoA synthase/ligase
381 (LACS), an enzyme that does not act on fatty acids of less than 12 C-atoms (Wu et al., 2020).
382 However, different types of fatty acyl CoA synthases can be found to be more closely related to the
383 *Polytomella* enzyme using BLAST (45-50% ID), including medium chain acyl-CoA synthase and
384 even bacterial 3-methylmercaptopropionyl-CoA ligases. We thus changed the annotation of the
385 enzyme to fatty acyl-CoA synthase (FACS). This enzyme is the prime candidate for the production of
386 butyryl-CoA in *Polytomella* sp., pending further experimental confirmation. A true LACS isoenzyme
387 was also detected (UTR_g2481, FC 0.16), but since its expression level is much lower than FACS,
388 this enzyme is unlikely to act as the first step of butyrate assimilation. Two acyl CoA oxidases
389 (ACX) were also highly butyrate-specific, with a FC value of 0.001 for ACX4 and 0.021 for its
390 paralog ACX. ACX4 was predicted to be localized in the plastid but homologs in other algae
391 including *C. reinhardtii* retrieved by BLAST searches (~51% ID) are annotated as peroxisomal
392 (Table I). Examination of the N-terminus of isoform ACX reveals a typical PTS2 signal and shows
393 34% sequence identity to *C. reinhardtii* ACX2, which catalyzes the first step of peroxisomal fatty
394 acid β-oxidation in the green alga *C. reinhardtii* (Kong et al. 2017). These two ACX enzymes likely
395 oxidize butyryl-CoA into crotonyl-CoA, which is converted into 3-hydroxybutyryl-CoA and then
396 into acetoacetyl-CoA by respectively the enoyl-CoA hydratase and the hydroxyacyl-CoA
397 dehydrogenase activities of the multifunctional protein MFP (Fig. 6). Compared to ACX4, MFP was
398 found to be more modestly induced by butyrate (FC 0.1). The final step of β-oxidation is carried out
399 by acetoacetyl-CoA thiolase (ATO1, FC 0.004), converting acetoacetyl-CoA into two molecules of
400 acetyl-CoA.

401 All 4 identified enzymes have typical PTS peroxisome targeting signals (Table I) and are thus
402 confirmed to be peroxisomally targeted. The fatty acid β -oxidation pathway used by *Polytomella* sp.
403 is typical for algae and plants, where it is found in both mitochondria and peroxisomes (Kong et al.,
404 2017; Li-Beisson et al., 2019; Pan et al., 2020; Kato et al., 2021).
405 We currently have no data on a mitochondrial β -oxidation pathway in *Polytomella* sp., but our study
406 clearly indicates that the peroxisomal pathway is key in the assimilation of butyrate. The peroxisomal
407 β -oxidation pathway of butyrate in *Polytomella* sp. differs from that in non-photosynthetic organisms
408 and bacteria by the CoA activation step and by the presence of MFP. Besides the use of a FACS type
409 enzyme, CoA activation of butyrate in mammals and microorganisms and can also use a butyrate-
410 CoA ligase/synthetase (EC 6.2.1.2) (De Preter et al., 2012). Conversely, fermentative butyrate
411 production from butyryl-CoA in bacteria mainly occurs via phosphate butyryltransferase (EC
412 2.3.1.19) + butyrate kinase (EC 2.7.2.7) (Walter et al., 1993) or butyryl-CoA:acetate CoA-transferase
413 (EC 2.8.3.8) (Duncan et al., 2002). The presence of a bifunctional MFP is the hallmark of
414 peroxisomal β -oxidation in plants, fungi and microalgae (Arent et al., 2010). In contrast, its two
415 reactions are carried out by separate enzymes in mitochondrial β -oxidation of butyrate in mammalian
416 colonocytes (De Preter et al., 2012).
417

418 **3.5.2 Glyoxylate cycle and citrate/malate shuttles**

419 The glyoxylate cycle comprises five enzymes which are mostly present in peroxisomes but some,
420 depending on the organism, can also be found in the cytosol, possibly to protect them from ROS-
421 induced damage. In *C. reinhardtii*, the glyoxylate cycle allows growth on acetate (Lauersen et al.,
422 2016) following its conversion into acetyl-CoA. Glyoxylate and acetyl-CoA are converted into
423 malate and further into citrate and succinate, which are exported to enter central carbon metabolism,
424 and can replenish the pool of TCA cycle intermediates. In *Polytomella*, the typical glyoxylate cycle
425 enzymes malate synthase (MAS1, FC 0.4) and isocitrate lyase (ICL1, FC 0.23) are induced on
426 butyrate, but at a lower level than citrate synthase (CIS2, FC 0.03) and malate dehydrogenase
427 (MDH2, FC 0.03) (Fig. 6). Aconitase (ACO) is also part of the cycle and three isoforms were
428 detected (suppl. Table I) but none were induced significantly by butyrate. MAS1 is confirmed to
429 localize in the peroxisome based on the presence of a typical PTS1 targeting signal at its C-terminus
430 (Gonzalez et al., 2011). CIS2 is predicted to be targeted to the peroxisome by DeepLoc (Almagro
431 Armenteros et al., 2017) (Table I) and its closest homologs are found in peroxisomes in plants and
432 yeast (Kunze et al., 2006; Rottensteiner and Theodoulou, 2006). *Polytomella* CIS2 and MDH2 show
433 highest amino acid sequence identities to peroxisomal/glyoxysomal-type homologs. ACO may also
434 be peroxisomal since three out of four amino acids of the consensus PTS2 signal are present (RV-X5-
435 RA instead of RV-X5-H/QA) (Gonzalez et al., 2011). In *C. reinhardtii*, only ICL was found in the
436 cytosol with the other 4 enzymes in peroxisomal microbodies (Lauersen et al., 2016). Earlier it was
437 found that in *Polytomella caeca*, microbodies separated from mitochondria on a sucrose gradient
438 contained MAS and a minor part of ICL activity, with most of it being cytosolic (Haigh and Beevers,
439 1964). Since these authors concluded that the ICL activity within the microbodies accounted for the
440 observed acetate assimilation, it may be assumed that ICL functions in the peroxisome, as is also
441 predicted by DeepLoc (Table I). The upregulation of ICL1 on butyrate with respect to acetate may
442 indicate an increased activity of the cycle, resulting in higher glyoxylate and succinate production.
443 While glyoxylate serves to produce malate via MAS in the peroxisome, succinate may be exported to
444 the cytosol and further imported into the mitochondria for use in the TCA cycle (Fig 6).
445 The pronounced increase of MDH2 may be related to the production of NADH by MFP during
446 butyrate β -oxidation in the peroxisome. At the expense of NADH, MDH2 can convert oxaloacetate
447 (OAA) into malate, which can be later exported to the cytosol (Fig. 6) via a malate/OAA transporter

448 (Rottensteiner and Theodoulou, 2006). Export of citrate produced by CIS2 from oxaloacetate is
449 likely occurring under butyrate growth considering the very strong induction of the cytosolic
450 ATP:citrate lyase (ACLY, FC 0.005). This enzyme produces acetyl-CoA and oxaloacetate from
451 citrate in the cytosol, thus allowing the export of acetyl-CoA. The oxaloacetate resulting from ACLY
452 can be re-imported to replenish the peroxisomal oxaloacetate pool for the proper functioning of the
453 glyoxylate cycle (Fig. 6). Despite the significant relatedness of MDH2 to its peroxisomal homolog in
454 *C. reinhardtii*, (62% amino acid identity) it can currently not be excluded that MDH2 is cytosolic,
455 and if so, this would indicate an increased need for malate/oxaloacetate shuttle activity to sustain
456 increased production and export of citrate from the peroxisome. A cytosolic localization for MDH,
457 ACO and ICL occurs in yeast and does not impact glyoxylate cycle function (Rottensteiner and
458 Theodoulou, 2006). The fact that MDH2 and CIS2 are more induced than ICL1 and MAS1 points to
459 an apparent increased need for a malate/oxaloacetate shuttle and citrate export in butyrate
460 metabolism. With regard to CIS, it was shown that during ^{14}C -acetate assimilation of *P. caeca*,
461 malate was by far the most important immediate product incorporating ^{14}C , with succinate and
462 (mitochondrial) fumarate 10-fold lower, but hardly any citrate was formed (Haigh and Beevers,
463 1964). Conversely, judged from the upregulation of CIS2 and ACLY, butyrate seems to specifically
464 induce peroxisomal citrate production. Since the outcome of butyrate utilization is the increased
465 production of acetyl-CoA in the cytosol from ACLY, an induction of fatty acid synthesis may be
466 expected in organelles. It is interesting that in human colonocytes, butyrate stimulates cell
467 proliferation via histone acetylation in the nucleus, involving the production of acetyl-CoA by ACLY
468 (Donohoe et al., 2012). In our study, no histone acetyltransferase was found differentially expressed.
469

470 3.5.3 Transporters and metabolite exchange

471 Relative to acetate, butyrate induced 10 membrane bound transporter proteins with significant
472 associated FC values (Table I, category “solute transport”), among which genuine peroxisomal
473 transporters. However, the identity of the proteins transporting butyrate or butyryl-CoA into the
474 peroxisomes remains uncertain. The ABCD transporter PXA (FC 0.1) shows high similarity to an
475 ABCD transporter in *C. reinhardtii* (A0A2K3CWL4/Cre15.g637761) which was confirmed to be
476 involved in the import of activated long-chain fatty acids from the cytosol to the peroxisomal matrix,
477 similar to the yeast peroxisomal ABC transporters PXA1 and PXA2 (Hettema et al., 1996). PXA
478 targets long-chain fatty acyl-CoA molecules, which butyryl-CoA is not, so its involvement in the
479 import of butyryl-CoA from the cytosol is uncertain. It might be necessary instead to channel CoA
480 into the peroxisome for CoA homeostasis. Potentially, the two cytosolic acetyl-CoA synthase-type
481 enzymes (ACSS) that were upregulated by butyrate (FC 0.08, 0.11) may provide substrates for this
482 process. Another induced transporter belongs to the PEX11 family (FC 0.09, category cell cycle in
483 Table I), a membrane protein that promotes peroxisome division in eukaryotes and is crucial for
484 medium-chain fatty acid (MCFAs) beta-oxidation. It was proposed that in yeast, PEX11 provides
485 MCFAs including butyrate to the peroxisome interior for CoA activation, effectively fulfilling a
486 transporter function (van Roermund et al., 2000). Two further proteins show clear homology to the
487 peroxisomal NAD carrier PXN (FC 0.155, 0.231) in *Arabidopsis thaliana*, which mediate the import
488 of NAD into peroxisomes against AMP (van Roermund et al., 2016). PXN belongs to the
489 mitochondrial carrier (TC 2.A.29) family, which contains also peroxisomal transporters. Butyrate
490 may thus increase the import of cofactors in the peroxisome, possibly linked to enhanced peroxisome
491 biogenesis.

492 Three proteins were identified as mitochondrial transporters, indicating also an involvement of
493 mitochondrial metabolism in butyrate utilization. Two of them are subunits of the mitochondrial
494 pyruvate transporter (MPC1, FC 0.08 & MPC2, FC 0.1), an oligomeric complex of approximately

495 150 kDa in the inner mitochondrial membrane which constitute the sole entry point into the
496 mitochondria of pyruvate, produced by glycolysis or from malate. The upregulation of this carrier is
497 of fundamental importance in establishing the metabolic programming of a cell (Bricker et al., 2012).
498 Once in the matrix, pyruvate can be converted into acetyl-CoA by the pyruvate dehydrogenase
499 complex (PDH) and feed the TCA cycle (McCommis and Finck, 2015). Cycle turnover produces
500 CO₂ and reducing power further used for ATP production, but intermediates can be siphoned off such
501 as citrate, which can exit the mitochondria and be cleaved back to acetyl-CoA and oxaloacetate by
502 ATP citrate lyase (ACLY) in the cytosol. Another transporter identified is homologous to the
503 mitochondrial dicarboxylate/tricarboxylate transporter DTC (FC 0.6) in *A. thaliana* (Millar and
504 Heazlewood, 2003). DTCs transport dicarboxylic acids (eg malate, oxaloacetate) and tricarboxylic
505 acids (eg citrate, isocitrate) into the mitochondrial matrix. In view of the FC value of 0.6, the role of
506 DTC is only modestly increased in butyrate metabolism, but the iBAQ value for DTC is highest
507 among transporters and represents one of the most abundant among butyrate induced proteins,
508 illustrating the importance of di/tricarboxylates for mitochondrial metabolism. Seeing that the levels
509 of the proteins of mitochondrial respiration (OXPHOS complexes) are not induced by butyrate, it can
510 be proposed that increased import of pyruvate and dicarboxylates feeds other metabolic pathways,
511 such as amino acid synthesis (see below).
512 Furthermore, two general substrate transporters of the Major Facilitator Superfamily were identified
513 (MFS, FC 0.2, 0.56). MFS transporters can only transport small solutes in response to chemiosmotic
514 ion gradients and can be found anywhere in the cell, so their proposed placement in the peroxisomal
515 membrane for transport of carboxylates is speculative (Fig 6). The monocarboxylate transporters
516 MCT that are known in humans to transport acetate and butyrate across the plasma membrane are
517 also members of the MFS family (Casal and Leão, 1995), but they are not orthologous to the two
518 MFS proteins mentioned above. Also, a typical MCT could not be found in the *Polytomella* sp.
519 genome. However, a member of the formate/nitrite transporter (TC 2.A.44) family (FNT, FC 0.21)
520 was found to be induced by butyrate. FNT transporters transport monovalent anions and are not
521 strictly selective as they can use nitrite or formate but also larger organic anions such as lactate and
522 acetate (Lu et al., 2012). It may thus be that this FNT is actually responsible for butyrate transport
523 over the plasma membrane in *Polytomella* sp. Further biochemical and genetic studies need to
524 confirm whether this is the case. Five genes belonging to the GPR1/FUN34/YaaH (GFY)
525 superfamily and homologous to bacterial acetate/succinate channels were found to be induced by
526 acetate in *C. reinhardtii* and possibly implicated in intracellular acetate transport (Durante et al.,
527 2019). In the *Polytomella* sp. genome, 4 GFY genes were identified of which only 1 (UTR_1663.t1)
528 was found in the proteome induced by butyrate at FC 0.636 (but with $p > 0.004$).
529 One transport protein is actually slightly downregulated, a P-type plasma membrane H⁺-ATPase
530 (PMA3, FC 3.9) that exports cellular protons (Morth et al., 2011). In *C. reinhardtii*, increased PMA
531 expression was found to improve tolerance to high CO₂ concentrations, which are toxic due to the
532 acidification of the cell interior (Choi et al., 2021). Acetate or butyrate are imported in the protonated
533 form and dissociate in the cytosol. It can be hypothesized that butyrate necessitates less expulsion of
534 H⁺ since it contains relatively fewer carboxylic acid groups at only 1 COOH per 4 C-atoms while
535 acetate contains 1 COOH per 2 C-atoms.

536

537 **3.5.4 Antioxidant defense**

538 Reactive oxygen species (ROS) are important in cellular signaling, but stress conditions may cause
539 increased ROS production and result in oxidative damage (Rezayian et al., 2019). Various
540 antioxidant defense systems to neutralize ROS exist in different cellular compartments, especially in
541 organelles that are major sources of ROS such as H₂O₂ (Roy et al., 2021). The butyrate metabolic

542 responses include a total of 10 proteins that are associated to antioxidant defense. One catalase
543 isoform, co-orthologous to the *C. reinhardtii* CAT1 isoform that localizes to peroxisomes (Kato et
544 al., 2021) and similarly endowed with a non-canonical C-terminal PTS1 signal (SVL), was found
545 markedly induced on butyrate (FC 0.003), while a second CAT1 ortholog was far less induced. No
546 clear ortholog was found for the *C. reinhardtii* ER-localized CAT2. Catalase upregulation probably
547 relates to the β -oxidation of butyrate, where it allows the detoxification of H_2O_2 produced by ACX
548 into H_2O and O_2 . Using density gradients, (Gerhardt, 1971) found the catalase and malate synthase
549 activities in different particulate fractions in *P. caeca*, which raised the question whether different
550 types of peroxisomes exist in the cell. A study to detect peroxisomes using CAT-specific staining
551 seemed to show that indeed different staining intensities existed in a sample of isolated peroxisomes
552 (Gerhardt and Berger, 1971).
553 Ascorbate peroxidase (APX, FC 0.015) was highly induced by butyrate. It is part of the glutathione-
554 ascorbate cycle (GAC) that uses electrons from NAD(P)H for the reduction of H_2O_2 to H_2O . Other
555 GAC enzymes were also induced on butyrate, such as glutathione S-transferase (GST3, FC 0.51),
556 while glutathione reductase (GR) was not. The GAC can be found in different cellular compartments
557 such as plastids, mitochondria, peroxisomes and the cytosol, (Caverzan et al., 2012). Since no
558 coherent targeting signals were found for *Polytomella* APX, GST3 and GR, the GAC was tentatively
559 placed in the cytosol in Fig. 6 since the closest homologs of these enzymes in *C. reinhardtii* are
560 predicted to be cytosolic. A typical 2-Cys peroxiredoxin (PRX2, FC 0.05) was found highly induced
561 on butyrate. PRXs are important for cellular redox signaling and antioxidant defense as they detoxify
562 organic hydroperoxides (R-O-OH) that can be formed from the reaction of organic molecules with
563 H_2O_2 (Liebthal et al., 2018). Another important ROS scavenging enzyme is superoxide dismutase,
564 which produces H_2O_2 from O_2^- . Two SOD isoforms were found, only modestly induced on butyrate
565 (MSD1, FSD1, FC 0.26, 0.34). The localization of PRX2 and M/FSD1 is uncertain as they lack
566 typical targeting signal and were predicted to be cytosolic by DeepLoc. Intriguingly, the levels of
567 plastid type alternative oxidase (PTOX, FC 0.43), which functions in plastid redox homeostasis by
568 oxidizing plastoquinol to reduce O_2 to H_2O in photosynthetic organisms (Krieger-Liszkay and Feilke,
569 2016), and the NAD(P)H dehydrogenase that feeds electrons into the plastoquinone pool (NDA2, FC
570 0.15), were higher on butyrate than acetate. This suggests a role of chlororespiration in antioxidant
571 defense in *Polytomella*. It is of note that these enzymes are found in the thylakoid membrane in *C.*
572 *reinhardtii*, while in *Polytomella* sp. a localization to the amyloplast envelope is proposed in absence
573 of a description of any intraplastidial membrane system (Fuentes-Ramírez et al., 2021).
574 Interestingly, photosynthesis in rice leaves was found to be protected due to a more efficient
575 antioxidant response when CAT and APX activity were limited, which was proposed to be because
576 of higher H_2O_2 levels that exert a positive regulatory influence (Sousa et al., 2019). First off, it would
577 be interesting to know whether the C4 fatty acid butyrate does in fact induce β -oxidation in
578 photosynthetic algae since it is known that *C. reinhardtii* favors membrane turnover over β -oxidation
579 in presence of exogenous C16 fatty acid (Kato et al., 2021). If not it would explain directly why
580 butyrate is poorly used by *C. reinhardtii* (Lacroux et al., 2020). If butyrate does enter β -oxidation,
581 increased CAT and APX could modify ROS levels and, in the view of (Sousa et al., 2019), interfere
582 with photosynthesis and hinder the growth on butyrate by green algae, as observed by (Lacroux et al.,
583 2020). *Polytomella* sp does not perform photosynthesis and is thus less affected by the very strong
584 antioxidant responses elicited by that the β -oxidation of butyrate, which is possibly at the basis of its
585 capacity to grow well on butyrate.
586

587 3.5.5 Branched chain amino acid degradation

588 A number of proteins induced on butyrate, placed in both the lipid and amino acid metabolism
589 categories (Table I), potentially participate in the degradation of branched chain amino acids
590 (BCAAs), by which valine is converted to propionyl-CoA, while degradation of isoleucine produces
591 both propionyl-CoA and acetyl-CoA (Fig. 7). This BCAA pathway is described in prokaryotes and in
592 eukaryotes such as mammals, yeasts and plants (Binder, 2010), but also in microalgae, for example
593 the diatom *Phaeodactylum tricornutum* (Pan et al., 2017) or *C. reinhardtii* (Liang et al., 2019). The
594 first enzyme of this pathway is branched-chain aminotransferase (BCA2, FC 0.28), probably located
595 in the mitochondria. Except for the second enzyme, branched-chain alpha-keto acid dehydrogenase
596 (BCKDC, FC 2.1), all enzymes in this pathway are induced by butyrate, in particular the central
597 enzyme methylmalonate semialdehyde dehydrogenase (MMSA, FC 0.005). Most of the downstream
598 enzymes seem to be targeted to the peroxisome in *Polytomella* sp. (Table I), recapitulating the
599 situation in plants where BCAA degradation starts in the mitochondrion to yield CoA-esterified
600 metabolites that are further converted in the peroxisome (Linka and Theodoulou, 2013).
601 Questions remain about this pathway in *Polytomella* sp. The pathway depends likely on the cellular
602 localization of MMSA. While the *C. reinhardtii* methylmalonate semialdehyde dehydrogenase
603 (ALDH6) is predicted to be mitochondrial, the *Polytomella* ortholog is predicted to be peroxisomal
604 (Fig. 7). If the latter is the case, the degradation of both isoleucine and valine towards acetyl-CoA can
605 occur unimpeded in the peroxisome. If we however entertain the possibility that MMSA is
606 mitochondrial in *Polytomella* sp., the situation is different. MMSA is able to convert MMS into
607 propionyl-CoA but also malonate semialdehyde (MS) into acetyl-CoA, so the degradation of
608 isoleucine into MS (via propionyl-CoA) does not demand the presence of MMSA in the peroxisome
609 when MS is imported into mitochondria. Mitochondrial MMSA can convert MS into acetyl-CoA
610 which can be further utilized without problems. In the case of valine degradation, the absence of
611 MMSA in the peroxisome would block the pathway at the level of the conversion of MMSA to
612 propionyl-CoA, and in that case MMS would have to be exported to the mitochondria. Here, MMSA
613 would convert MMS into propionyl-CoA, but its fate in the mitochondria would not be obvious: the
614 enzymes necessary for its conversion to succinyl-CoA (propionyl-CoA carboxylase producing (S)-
615 methylmalonate-CoA, methylmalonyl-CoA epimerase producing (R)-methylmalonate-CoA and
616 methylmalonyl-CoA mutase to convert it to succinyl-CoA) could not be identified in the *Polytomella*
617 genome. This is similar to the case of *P. tricornutum* where the epimerase step was not detected (Pan
618 et al., 2017). In *P. caeca* cells grown on propionate, propionyl-CoA carboxylase activity could not be
619 detected (Lloyd et al., 1968). The same is true in plants, unlike in mammals and bacteria (Linka and
620 Theodoulou, 2013). The TCA cycle enzyme succinyl-CoA ligase (SCL, FC 0.77 at $p > 0.003$),
621 somewhat induced by butyrate, was found to be a promiscuous enzyme that produces also thioesters
622 of malate, fumarate and glutarate among others (Nolte et al., 2014). It may be hypothesized that SCL
623 can produce succinyl-CoA directly from methylmalonate semialdehyde (MMS). Alternatively, MMS
624 may also be imported into mitochondria and converted into malonate by an aldehyde dehydrogenase
625 (ALD5 EC:1.2.1.-; at least 5 enzymes are found in the proteome, suppl. Table I) and then further into
626 malonyl-CoA via malonate ligase (ACSF3, FC 0.38 but with $p > 0.004$), which serves as precursor for
627 fatty acid synthesis (see 3.5.6). It is noted that even if ALD5/ACSF3 are not located in the
628 mitochondria, the products can be imported into the organelle. Alternatively, the BCAA degradation
629 pathway may be streamlined when MMSA is dually targeted to both peroxisome and mitochondria,
630 which is known for other enzymes such as CAT (Petrova et al., 2004).
631 In the non-sulfur purple bacterium *Rhodospirillum rubrum*, which does not possess a glyoxylate
632 cycle, the BCAA degradation pathway was identified as assimilatory during growth on butyrate (De
633 Meur et al., 2020). Interestingly, *R. rubrum* grew 3-fold faster in presence of HCO_3^- , which serves as
634 electron sink and helps antioxidant defense. However, since *Polytomella* sp. does possess an active

635 glyoxylate cycle, the purpose of the BCAA degradation pathway in butyrate assimilation is not
636 directly obvious. It could serve to produce propionyl-CoA for metabolic pathways such as the
637 synthesis of coenzyme A. Leucine degradation has been found in *A. thaliana* alongside starch and
638 lipid degradation in response to stress conditions that perturb cellular energy balance, such as
639 senescence and carbon deprivation (Mentzen et al., 2008). In these conditions, it is conceivable that
640 the cell makes up for a lack of energy and carbon by mobilizing internal reservoirs of sugar, lipid and
641 amino acids. In *Polytomella*, all three are observed in cells growing on butyrate (see 3.5.6), whereby
642 sugars and lipids may serve to produce amino acids such as BCAAs. We propose that butyrate is
643 metabolized and yields acetyl-CoA and further di/tricarboxylic acids at a slower rate than acetate,
644 which is compensated for by the degradation of BCAAs to produce acetyl-CoA and possibly
645 succinyl-CoA that feed into carbon metabolism. A factor in the induction of the BCAA degradation
646 pathway specifically may be the fact that it shares several enzymes with the β -oxidation of butyrate
647 (ACX, MFP, ATO).
648

649 **3.5.6 Catabolic production and role of pyruvate**

650 Pyruvate is at the crossroads of many metabolic pathways and is important in all cells and cell
651 compartments (Shtaida et al., 2015). There are multiple indications that butyrate metabolism goes
652 also through pyruvate, while it is not predicted to be directly involved in acetate utilization. First,
653 most enzymes of glycolysis are upregulated several fold under butyrate, including pyruvate kinase
654 (PYK1, FC 0.13) (Table I), which should result in increased pyruvate production and ATP.
655 Compared to acetate, the balance seems to be shifted towards starch and glucose degradation, in line
656 with the cellular sugar content being lower on butyrate (Fig. 1D) and the induction of the
657 mitochondrial MPC transporter for pyruvate (see 3.5.3). This may not be leading to higher TCA
658 cycle and OXPHOS activities since the necessary proteins are not induced, but pyruvate may instead
659 be converted into amino acids such as alanine, and fatty acids (see below). Also, pyruvate
660 decarboxylase (PDC3, FC 0.14) was induced, which should lead to acetaldehyde production in the
661 cytosol. This could diffuse through the mitochondrial membrane and then be converted into acetate
662 by NAD⁺ aldehyde dehydrogenase (ALD5, FC 0.03) and then acetyl-CoA by acetyl-CoA synthase
663 (ACSS, FC 0.01). This scenario is supported by the fact that *Polytomella caeca* can grow on
664 acetaldehyde (1mM) as sole external carbon source (Wise, 1968). It cannot be excluded that
665 acetaldehyde is converted into acetate in the cytosol which is then imported into the mitochondria
666 (see 3.5.8). Finally, there may also be a contribution from NADP malic enzyme (ME, FC 0.82 with
667 $p > 0.004$) converting malate to pyruvate in the cytosol. Since this enzyme was predicted to be
668 targeted to the plastid, it can provide a source of pyruvate from imported malate. Via an MDH type
669 enzyme (5 different MDH were detected in the proteome, suppl. Table I) in the plastid that produces
670 NADH, malate may also feed the PTOX enzyme that was found induced on butyrate (see 3.5.4) and
671 is implicated in maintaining cellular redox balance. Indeed, 2 MDH enzymes and PTOX were
672 detected in a proteomics study of isolated non photosynthetic plastids from *Polytomella parva*
673 (Fuentes-Ramírez et al., 2021). Pyruvate is also at the basis for the production of coenzyme A and
674 NAD⁺, with pantoate:beta-alanine ligase (PANC, FC 0.21) of the CoA/ACP synthesis pathway and
675 quinolinate synthase (QS, FC 0.62) of the NAD⁺ synthesis increased, suggesting a need of CoA/ACP
676 in butyrate metabolism.
677 A clear upregulation is found of two of the four enzymes of the type II fatty acid synthesis (FAS)
678 system, which uses an acyl carrier protein (ACP): 3-oxoacyl-ACP reductase (fabG, FC 0.006) and
679 enoyl-ACP reductase (MECR, FC 0.184). In *C. reinhardtii*, the four different subunits of the type II
680 FAS system are predicted to be dually targeted to the mitochondrion and chloroplast, similar to
681 plants (Riekhof et al., 2005; Li-Beisson et al., 2013). Fatty acids produced in the plastid are used for

682 the production of membranes, storage and signaling lipids (Li-Beisson et al., 2015). The FAs are
683 unlikely to be destined for the production of storage lipids since levels are actually lower in butyrate
684 grown cells (Fig. 1D). Fatty acids produced by mitochondrial (mt)FAS play various roles. The
685 mtFAS pathway fuels the production of acyl-ACPs including octanoyl-ACP, which is a precursor of
686 lipoic acid, a cofactor of several metabolic enzymes: pyruvate dehydrogenase (PDH), α -ketoglutarate
687 dehydrogenase (KGDH), branched-chain α -ketoacid dehydrogenase (BCKDH), the glycine
688 decarboxylase complex (GDC), and plastidial pyruvate dehydrogenase (ptPDH) (Guan et al., 2020).
689 Four out of five of these enzymes are indeed upregulated on butyrate with FC values of 0.58-0.87,
690 and although these values are not statistically sound enough to warrant inclusion in Table I, it does
691 represents a clear trend. Paradoxically, the only enzyme not changed is BCKDH, which is involved
692 in the BCAA degradation pathway that is highly expressed on butyrate. This suggests that the
693 pathway is not regulated at the level of this enzyme, which is not an uncommon observation in
694 biochemical studies (eg Nogaj et al., 2005). The mtFAS system is possibly induced to provide acyl-
695 ACPs to two enzymes involved in biotin synthesis, 3-oxoacyl-ACP reductase (OAR, FC 0.06 and 7-
696 keto-8-aminopelargonic acid synthase (KAPAS, FC 0.016), which uses pimeloyl-ACP as substrate.
697 Biotin is known to be a cofactor of certain carboxylase enzymes, including acetyl-CoA carboxylase
698 (ACC) which functions 2 steps upstream of the FAS system producing malonyl-CoA from acetyl-
699 CoA. ACC was the only enzyme with a biotin cofactor that was detected in the *Polytomella*
700 proteome, and although it is not induced by butyrate it may be regulated post-translationally. It is
701 noted that ACLY in the cytosol is strongly induced (see 3.5.2) and produces the acetyl-CoA that is a
702 direct substrate for ACC. Biotin has been described to exert regulatory influences in cell signaling,
703 for example the upregulation of glucose metabolism (Dakshinamurti, 2005), which was indeed
704 induced on butyrate.

705

706 **3.5.7 Metabolic activities on acetate**

707 The differential approach revealed that the proteins more abundant on acetate than on butyrate tend to
708 relate to the protein biosynthesis and homeostasis (further referred to as proteostasis) rather than to
709 specific metabolic pathways. Among the over-represented categories are "RNA processing" and
710 "Protein biosynthesis, modification and homeostasis". This includes heat-shock proteins, protein
711 kinases, maturation-, elongation- and assembly factors. Although butyrate induced more proteins
712 compared to acetate, there may also be downregulation signals produced in response to specific
713 metabolic needs imposed by butyrate. A specific perception of an acetate-linked metabolite and
714 associated signal cascades may also be involved. Some of the proteins suppressed by butyrate may
715 suggest the implication of a mitogen-activated protein kinase (MAPKs) signal transduction pathway,
716 which modulates important cellular processes such as proliferation, stress responses, apoptosis and
717 immune defense via consecutive protein phosphorylations by serine and threonine protein kinases
718 (Soares-Silva et al., 2016).

719 We note the induction of a protein of uncertain function, being either protein kinase (MAP3K-RAF)
720 or dual specificity kinase splA isoform B (FC 4.663). It may suggest activation of a signal
721 transduction pathway for positive regulation of gene transcription from a receptor on the cell surface
722 (Soares-Silva et al., 2016). The presence of a PPP Fe-Zn-dependent phosphatase (FC 1.8) involved in
723 reversible protein posttranslational modification points also in this direction. Cytosolic Hsp70
724 chaperone (FC 12.422) may also be involved in this MAPK signaling pathway, as is the case in
725 mammals (Fan et al., 2018). GTPase activating component Ran-GAP (FC 2.862) is also known to be
726 implicated downstream of MAPK responses (Faustino et al., 2007). A number of proteins involved in
727 different stages of synthesis and maturation of RNAs and proteins are found. This includes the
728 mitochondrial Tr-type G domain-containing GTPase/elongation factor Tu (FC 8.245) which bring the

729 aminoacyl-tRNA into the A site of the mitoribosome, and Nsa1/WDR74 (FC 3.966), an assembly
730 factor involved in the maturation of the large subunit of the cytosolic ribosome. The only ribosomal
731 protein that is overaccumulated is RPL38, suggesting that it performs an additional function. Several
732 proteins involved in the biogenesis and maturation of mRNA and ribosomes are found at FC values
733 of 2-3, which are at the 'executive' side of signal transduction pathways that end in protein synthesis
734 (Table I).

735 Of note are the three plastidial small heat shock proteins (HSP20, FC 12.510, 10.588, 6.530) for
736 which little data exist in microalgae but in plants play a central role in the protection against stress
737 damage, in the folding, intracellular distribution, and degradation of proteins, as well as in signal
738 transduction chains (Ouyang et al., 2009). The HSPs are known to be generally involved in the
739 response to stress most notably due to heat, but also other stresses that can affect protein stability
740 such as oxidative stress, salinity or pH (Strauch and Haslbeck, 2016). Acetate is more likely than
741 butyrate to be transported across the cell and imported into organelles to give rise to acetyl-CoA and
742 further biosynthesis reactions (Boyle et al., 2017). Butyrate is likely only taken up in the peroxisome
743 and di/tricarboxylates are exported into the cytoplasm and further into organelles. Since acetate is
744 transported in the protonated form it will systematically release H⁺ within the organelles, which may
745 cause some level of stress and possibly explain the increased need for HSP20.

746 The mitochondrial organization/maturation factor (CHCH domain) (FC 16.131) is the most induced
747 protein compared to butyrate. Its function is uncertain, but may relate to protein translation or post-
748 translational maturation of cytochrome c oxidase. Finally, although most enzymes involved in amino
749 acid synthesis were mildly induced by butyrate, a few enzymes involved in production of aromatic
750 amino acids and methionine were more abundant on acetate (FC ~2.5). Methionine is a direct
751 precursor of S-adenosylmethionine (SAM), an important posttranslational regulator of many cellular
752 processes, including autophagy, the recycling of cellular components in response to stress (Ouyang et
753 al., 2020). Butyrate induction of proteins such as the stress-induced carboxypeptidase (SCPL, FC
754 0.47) (Xu et al., 2021) and universal stress protein (IMP2, FC 0.34) seem to indicate that butyrate
755 indeed causes some level of stress to the cells. It may thus be hypothesized that butyrate causes a
756 decrease methionine to lower SAM, since it inhibits processes involved in stress response such as
757 autophagy.

758

759 4 Conclusions and perspectives

760 The key hypotheses that have been proposed in the past concerning limitations in the trophic
761 metabolism of microalgae relate to cell permeability, toxic products formed from the substrate, lack
762 of enzymes necessary for effective dissimilation of the substrate or their improper cellular location,
763 lack of transcriptional control, effect of low-intensity light in stimulating heterotrophic growth and
764 respiratory deficiency, etc. (Neilson and Lewin, 1974). In this work, these key hypotheses were
765 considered with regard to butyrate assimilation in *Polytomella* sp., and the relation with butyrate
766 metabolism in other organisms is discussed as well as the potential implications of these findings for
767 the capacities for butyrate assimilation of other -green- algae. In addition, a major step has been made
768 in our understanding of peroxisomes in *Polytomella* sp. and in relation to its close relative *C.*
769 *reinhardtii*.

770 Based on our data, we propose that butyrate is assimilated via peroxisomal β -oxidation resulting in
771 acetyl-CoA and di/tricarboxylates for cellular use via the glyoxylate cycle. We found that multiple
772 transporters are induced to facilitate the metabolic interplay between peroxisome and other cell
773 compartments. Although no monocarboxylate transporter was identified for butyrate transport, a
774 formate/nitrite transporter was put forward as candidate for this function. We hypothesize that
775 butyrate causes a major antioxidant defense response related to the production of H₂O₂ and NADH in

776 β -oxidation. An increased turnover of BCAAs to propionyl-CoA and acetyl-CoA was suggested,
777 which may, together with an overproduction of pyruvate from glycolysis, serve amino acid or
778 cofactor production. Butyrate lowers accumulation of carbohydrates and lipids while fatty acid
779 synthesis was found induced, probably in the mitochondria. This all may serve organellar
780 reorganization (peroxisomes) and the production of cofactors for several central metabolic enzymes
781 to accommodate butyrate utilization. In contrast, acetate utilization seems to stimulate activities that
782 relate to the biosynthesis and homeostasis of proteins.
783 Its fast butyrate assimilation makes *Polytomella* sp. a good model for the study of VFA metabolism,
784 but the high starch levels even during the exponential growth is another distinctive trait that allow
785 continuous cultivation on dark fermentation effluents with potential for biofuel production. Our
786 proteomics approach revealed in many instances the induction on butyrate of multiple proteins
787 belonging to the same pathway or similar metabolic activities suggest their importance in butyrate
788 metabolism. Other omics and biochemical approaches should be employed to further explore the
789 specificities of butyrate vs acetate as a carbon source. In particular, metabolomics and fluxomics
790 should be used to reveal the assimilation pathways. The main issues that remain to be tackled relate
791 to the import of VFAs into the cell and the role of β -oxidation and associated antioxidant activities,
792 especially in green algae. As a non-photosynthetic alga, *Polytomella* can serve as a metabolic
793 reference for efficient butyrate assimilation, to which other (green) algae may be compared. Since
794 *Polytomella* sp. does not seem to appear to possess novel metabolic capacities *per se*, it should be
795 considered that this alga owes its fast butyrate assimilation in some way to the loss of another major
796 metabolic capacity: photosynthesis.
797

798 5 Tables

799 **Table I.** Overview of the most pertinent proteins with significant FoldChange values arranged by
800 metabolic category as determined by Mercator. PTS, presence of peroxisome targeting signal;
801 Loc_Chltre, location (when discordant) and accession no. of *C. reinhardtii* ortholog. Proteins
802 corresponding to the E-values are given in the suppl. Table I.

10	Redox homeost.	catalase	CAT1	utr_g8710.t1	56775	0	K03781	1.11.1.6	Px	O		64.78	0.003	-8.52	24745	23593495
10	Redox homeost.	ascorbate peroxidase	APX	utr_g2687.t1	40358	1.55E-139	K00428	1.11.1.5	Mt	PI	Cy_A0A2K3DF40	68.36	0.015	-6.10	473262	26685874
10	Redox homeost.	glutathione S-transferase	GST3	utr_g3599.t1	24935	3.91E-45	K04097	5.3.99.2	Cy	O		24.09	0.480	-1.06	788574	1341820
10	Redox homeost.	typical 2-Cys peroxidoxin	PRX2	utr_g3953.t1	21767	3.52E-117	K03386	1.11.1.24	Cy	O		30.2	0.049	-4.35	31157	1730222
10	Redox homeost.	Fe-Mn superoxide dismutase	MSD1	utr_g3322.t1	24515	5.98E-121	K04564	1.15.1.1	Cy	O	Mt_Q42684	58.26	0.261	-1.94	3886744	12236356
10	Redox homeost.	Fe-Mn superoxide dismutase	FSD1	utr_g7353.t1	38647	4.49E-94	K04564	1.15.1.1	PI	Mt	PL_A8IGH1	16.62	0.338	-1.57	542608	1312085
13	Cell cycle org.	peroxisomal fission factor	PEX11	utr_g5823.t1	25944	3.00E-89	K13352	-	Px	O		45.68	0.088	-3.51	3687867	34479357
15	RNA biosynthesis	transcription elongation factor	SPT5	utr_g7362.t1	115452	1.04E-129	K15172	-	Nc	O		4.53	2.751	1.46	118157	22315
16	RNA processing	mRNA-binding regulatory factor	RBP	utr_g1967.t1	35829	1.53E-66	K13201	-	Cy	O		10.09	2.407	1.27	385557	97577
16	RNA processing	trimethylguanosine synthase	TGS	utr_g6581.t1	116398	1.48E-46	K14292	2.1.1.-	Nc	O		3.97	3.049	1.61	67256	0
17	Prot. biosynthesis	Tr-type G domain-containing GTPase/elongation factor Tu	TYPB	utr_g3770.t1	80301	0	K06207	-	PI	Mt		6.01	8.245	3.04	146308	4416
17	Prot. biosynthesis	assembly factor Nsa1/WDR74	NSA1	utr_g7089.t1	53992	4.48E-56	K14841	-	Nc	O		4.69	3.966	1.99	127446	0
17	Prot. biosynthesis	GTPase assembly factor	LSG1	utr_g3801.t1	75849	1.37E-93	K14539	3.6.1.-	Cy	PI		10.3	2.564	1.36	287224	94147
17	Prot. biosynthesis	LSU proteome.component RPL38	RPL38	utr_g8236.t1	7805	1.18E-26	K02923	-	CY	PI		59.42	2.529	1.34	44287473	14828116
17	Prot. biosynthesis	pre-rRNA processing factor	FCF2	utr_g3144.t1	27799	8.18E-38	-	-	Nc	O		5.76	2.230	1.16	147997	0
18	Prot. modification	protein kinase (MAP3K-RAF)/Dual specificity kinase splA isoform B	SPLA	utr_g6123.t1	55422	0	K17535	2.7.11.1	Cy	O		2.21	4.663	2.22	108763	0
18	Prot. modification	PPP Fe-Zn-dependent phosphatase families.PP7-class phosphatase	PP7	utr_g2423.t1	61968	4.29E-134	K04460	3.1.3.16	Cy	O		3.06	1.755	0.81	50923	0
18	Prot. modification	class theta glutathione S-transferase	GST	utr_g5659.t1	31372	1.61E-53	K00799	2.5.1.18	Cy	SP		68.79	0.246	-2.02	16153692	54177371
19	Prot. homeostasis	mitochondrial organisation/ maturation factor (CHCH domain)	CHCH	utr_g75.t1	17083	1.99E-25	-	-	Mt	PI		16.96	16.13	4.01	2557159	0
19	Prot. homeostasis	plastidial small heat shock proteins	HSP22A	g5306.t1	21101	5.98E-26	K13993	-	Mt	O		33.51	12.51	3.64	982817	0
19	Prot. homeostasis	plastidial small heat shock proteins	HSP22A	utr_g2186.t1	21122	3.29E-29	K13993	-	Mt	O		20.21	10.58	3.40	757049	0
19	Prot. homeostasis	cytosolic Hsp70 chaperone system.chaperone (Hsp70)	HSP70A	utr_g6948.t1	72239	0.00E+00	K03283	-	Cy	O		31.91	12.42	3.63	716967	36532
19	Prot. homeostasis	plastidial small heat shock proteins	HSP22A	utr_g2897.t1	20969	7.72E-29	K13993	-	Mt	O		26.06	6.530	2.71	627450	0
19	Prot. homeostasis	S10-class serine carboxypeptidase	SCPL	utr_g3766.t1	55945	2.18E-167	K09645	3.4.16.-	SP	SP		30.18	0.468	-1.09	2321242	4070954
23	Prot. translocation	GTPase activating component Ran-GAP	RAN	utr_g2135.t1	55934	5.95E-122	K14319	-	Cy	O		18.55	2.862	1.52	426898	124086
24	Solute transport	P3A-type proton-translocating ATPase.plasma membrane	PMA3	utr_g4794.t1	134485	0.00E+00	K01535	7.1.2.1	Lys/	O		1.69	3.934	1.98	56952	0
24	Solute transport	MPC pyruvate carrier complex.component MPC1	MPC1	utr_g3777.t1	12923	1.07E-51	K22138	-	Mt	O		69.94	0.084	-3.58	2415540	23853875
24	Solute transport	MPC pyruvate carrier complex.component MPC2	MPC2	utr_g6536.t1	13329	1.24E-48	K22139	-	Mt	O		63.64	0.102	-3.30	1538010	12379886
24	Solute transport	ABC1 family.subfamily ABCD transporter	PXA	utr_g4304.t1	96371	0.00E+00	K05677	-	Mt	Mt	Px_A0A2K3CWL4	12.42	0.101	-3.31	110029	856155
24	Solute transport	mitochondrial substrate carrier protein (eg 2-oxodicarboxylate)	MCP26	utr_g1761.t1	36177	4.13E-123	K15110	-	Mt	Mt		26.01	0.101	-3.31	318737	2577120
24	Solute transport	peroxisomal nicotinamide adenine dinucleotide carrier	PXN	utr_g5259.t1	45068	8.88E-117	K13354	-	Px	SP		12.44	0.155	-2.69	72726	361502
24	Solute transport	Formate/nitrite transporter	FNT	utr_g7576.t1	33602	5.31E-93	K21993	-	Mb	O		8.63	0.209	-2.26	0	322350
24	Solute transport	Major Facilitator Superfamily general substrate transporter	MFS	utr_g3064.t1	57919	2.90E-114	K02532	-	ER	O		19.46	0.199	-2.33	1058783	4383133
24	Solute transport	peroxisomal nicotinamide adenine nucleotide transporter	PXN	utr_g4054.t1	36674	1.87E-59	K13354	-	Px	Mt		48.7	0.231	-2.11	3756544	13327162
24	Solute transport	MFS transporter (double), DHA1 family, multidrug resistance protein	MFS	utr_g3468.t1	59653	2.77E-101	K08157	-	Mb	SP	Fungal type	5.93	0.555	-0.85	2852646	4200884
24	Solute transport	mitochondrial dicarboxylate/ tricarboxylate transporter	DTC	g4183.t1	31891	2.53E-171	K15104	-	Mt	O		74.58	0.587	-0.77	86826580	12128351
26	External stimuli	carbonic anhydrase	CAH7	utr_g1251.t1	31431	8.71E-112	K01673	4.2.1.1	Cy	O		18.71	0.530	-0.92	405506	628951
35	Not assign.Annot.	glutathione S-transferase	GST	utr_g6818.t1	24782	2.17E-42	K04097	2.5.1.18	Cy	O		56.11	3.441	1.78	13437380	3219027
35	Not assign.Annot.	universal stress protein family/sugar utilization regulatory protein	IMP2	utr_g1902.t1	15369	8.52E-34	-	-	Cy	O		33.1	0.344	-1.54	2071937	4958676
35	Not assign.Annot.	Peroxisomal membrane protein	PMP22	utr_g2705.t1	8360	1.49E-09	K13347	-	Mt	O		25.64	0.379	-1.40	0	685316
35	Not assign.Annot.	isochorismatase	ISOC	utr_g326.t1	22040	5.79E-80	-	3.3.2.1	Cy	O		52.97	0.290	-1.78	8432129	23785614
35	Not assign.Annot.	CoA binding domain (succinyl CoA synthetases, malate/ATP-citrate	CoA_b	g2015.t1	17476	3.80E-54	K06929	-	Cy	O		43.4	0.204	-2.30	1387764	5645525
35	Not assign.Annot.	acetyl-CoA synthetase/acyl-activating enzyme 17	ACAS	utr_g327.t1	150268	6.21E-98	K01895/	6.2.1.1/3	Px	O	PTS1	6.89	0.051	-4.29	16375	264231
35	Not assign.Annot.	serine hydrolase (eg DHFR)	FSH1	utr_g7336.t1	36143	2.10E-36	-	--	Cy	O		25.3	0.053	-4.25	0	622170

804 **6 Conflict of Interest**

805 The authors declare that the research was conducted in the absence of any commercial or financial
806 relationships that could be construed as a potential conflict of interest.

807 **7 Author Contributions**

808 JL performed experiments, data acquisition, data curation, formal analysis and writing of the original
809 draft. AA contributed to conceptualization, experiments, data acquisition, data curation, formal
810 analysis, validation, review and editing of the original draft. SB performed experiments, data
811 acquisition, data curation and formal analysis. YC performed data acquisition, data curation, formal
812 analysis, validation, review and editing of the original draft. OV performed data acquisition, data
813 curation, formal analysis, validation, review and editing of the original draft. JPS contributed to
814 supervision, funding acquisition, validation, review and editing of the original draft. RVL designed
815 original experimental plan and performed experiments, data acquisition, data curation, formal
816 analysis, supervision, funding acquisition, validation, review and editing of the original draft. All
817 authors approved the final version of the manuscript.

818 **8 Funding**

819 JL received a PhD fellowship from European Union from the Occitanie region, France, with
820 complementary funding from FEDER. This study was funded by the National Institute of
821 Agriculture, Alimentation and Environment (INRAE), the CNRS, and was supported by the
822 FermALip project, funded by the Carnot institute 3BCAR as well as by the “Initiative d’Excellence”
823 program from the French State (Grant ‘DYNAMO’, ANR-11-LABX-0011-01). The proteomic
824 experiments were partially supported by Agence Nationale de la Recherche under projects ProFI
825 (Proteomics French Infrastructure, ANR-10-INBS-08) and by GRAL, a program from the Chemistry
826 Biology Health (CBH) Graduate School of University Grenoble Alpes (ANR-17-EURE-0003).

827 **9 References**

- 828 Acién Fernández, F. G., Fernández Sevilla, J. M., and Molina Grima, E. (2019). “Costs analysis of
829 microalgae production,” in *Biofuels from Algae* (Elsevier), 551–566. doi: 10.1016/B978-0-444-
830 64192-2.00021-4.
- 831 Adams, C., Godfrey, V., Wahlen, B., Seefeldt, L., and Bugbee, B. (2013). Understanding precision
832 nitrogen stress to optimize the growth and lipid content tradeoff in oleaginous green microalgae.
833 *Bioresour. Technol.* 131, 188–194. doi: 10.1016/j.biortech.2012.12.143.
- 834 Alban, C., Job, D., and Douce, R. (2000). BIOTIN METABOLISM IN PLANTS. *Annu. Rev. Plant*
835 *Physiol. Plant Mol. Biol.* 51, 17–47. doi: 10.1146/annurev.arplant.51.1.17.
- 836 Almagro Armenteros, J. J., Sønderby, C. K., Sønderby, S. K., Nielsen, H., and Winther, O. (2017).
837 DeepLoc: prediction of protein subcellular localization using deep learning. *Bioinformatics* 33,
838 3387–3395. doi: 10.1093/bioinformatics/btx431.
- 839 Arent, S., Christensen, C. E., Pye, V. E., Nørgaard, A., and Henriksen, A. (2010). The
840 Multifunctional Protein in Peroxisomal β -Oxidation. *J. Biol. Chem.* 285, 24066–24077. doi:
841 10.1074/jbc.M110.106005.
- 842 Binder, S. (2010). Branched-Chain Amino Acid Metabolism in *Arabidopsis thaliana*. *Arab. B.* 8,
843 e0137. doi: 10.1199/tab.0137.
- 844 Bouyssié, D., Hesse, A.-M., Mouton-Barbosa, E., Rompais, M., Macron, C., Carapito, C., et al.
845 (2020). Proline: an efficient and user-friendly software suite for large-scale proteomics.

- 846 *Bioinformatics*. doi: 10.1093/bioinformatics/btaa118.
- 847 Boyle, N. R., Sengupta, N., and Morgan, J. A. (2017). Metabolic flux analysis of heterotrophic
848 growth in *Chlamydomonas reinhardtii*. *PLoS One* 12, 1–23. doi: 10.1371/journal.pone.0177292.
- 849 Bricker, D. K., Taylor, E. B., Schell, J. C., Orsak, T., Boutron, A., Chen, Y.-C., et al. (2012). A
850 Mitochondrial Pyruvate Carrier Required for Pyruvate Uptake in Yeast, *Drosophila*, and
851 Humans. *Science* (80-.). 337, 96–100. doi: 10.1126/science.1218099.
- 852 Casabona, M. G., Vandenbrouck, Y., Attree, I., and Couté, Y. (2013). Proteomic characterization of
853 *Pseudomonas aeruginosa* PAO1 inner membrane. *Proteomics* 13, 2419–23. doi:
854 10.1002/pmic.201200565.
- 855 Casal, M., and Leão, C. (1995). Utilization of short-chain monocarboxylic acids by the yeast
856 *Torulaspora delbrueckii*: Specificity of the transport systems and their regulation. *BBA - Mol.*
857 *Cell Res.* 1267, 122–130. doi: 10.1016/0167-4889(95)00067-3.
- 858 Caverzan, A., Passaia, G., Rosa, S. B., Ribeiro, C. W., Lazzarotto, F., and Margis-Pinheiro, M.
859 (2012). Plant responses to stresses: Role of ascorbate peroxidase in the antioxidant protection.
860 *Genet. Mol. Biol.* 35, 1011–1019. doi: 10.1590/S1415-47572012000600016.
- 861 Chalima, A., Oliver, L., Fernández de Castro, L., Karnaouri, A., Dietrich, T., and Topakas, E. (2017).
862 Utilization of Volatile Fatty Acids from Microalgae for the Production of High Added Value
863 Compounds. *Fermentation* 3, 54. doi: 10.3390/fermentation3040054.
- 864 Choi, H. Il, Hwang, S. W., Kim, J., Park, B., Jin, E. S., Choi, I. G., et al. (2021). Augmented CO₂
865 tolerance by expressing a single H⁺-pump enables microalgal valorization of industrial flue gas.
866 *Nat. Commun.* 12, 1–16. doi: 10.1038/s41467-021-26325-5.
- 867 Craig, R. J., Hasan, A. R., Ness, R. W., and Keightley, P. D. (2021). Comparative genomics of
868 *Chlamydomonas*. *Plant Cell* 33, 1016–1041. doi: 10.1093/plcell/koab026.
- 869 Cuff, M., Dyer, J., Jones, M., and Shirazi-Beechey, S. (2005). The human colonic monocarboxylate
870 transporter Isoform 1: Its potential importance to colonic tissue homeostasis. *Gastroenterology*
871 128, 676–686. doi: 10.1053/j.gastro.2004.12.003.
- 872 Dakshinamurti, K. (2005). Biotin - A regulator of gene expression. *J. Nutr. Biochem.* 16, 419–423.
873 doi: 10.1016/j.jnutbio.2005.03.015.
- 874 Davidi, L., Levin, Y., Ben-Dor, S., and Pick, U. (2014). Proteome Analysis of Cytoplasmatic and
875 Plastidic β -Carotene Lipid Droplets in *Dunaliella bardawil*. *Plant Physiol.* 167, 60–79. doi:
876 10.1104/pp.114.248450.
- 877 De Duve, C., and Baudhuin, P. (1966). Peroxisomes (microbodies and related particles). *Physiol.*
878 *Rev.* 46, 323–357. doi: 10.1152/physrev.1966.46.2.323.
- 879 de la Cruz, V. F., and Gittleson, S. M. (1981). The genus *Polytomella*: A review of classification,
880 morphology, life cycle, metabolism, and motility. *Arch. fur Protistenkd.* 124, 1–28. doi:
881 10.1016/S0003-9365(81)80001-2.
- 882 De Meur, Q., Deutschbauer, A., Koch, M., Bayon-Vicente, G., Cabecas Segura, P., Wattiez, R., et al.
883 (2020). New perspectives on butyrate assimilation in *Rhodospirillum rubrum* S1H under
884 photoheterotrophic conditions. *BMC Microbiol.* 20, 1–20. doi: 10.1186/s12866-020-01814-7.
- 885 De Preter, V., Arijs, I., Windey, K., Vanhove, W., Vermeire, S., Schuit, F., et al. (2012). Impaired
886 butyrate oxidation in ulcerative colitis is due to decreased butyrate uptake and a defect in the
887 oxidation pathway*. *Inflamm. Bowel Dis.* 18, 1127–1136. doi: 10.1002/ibd.21894.
- 888 Delrue, F., Álvarez-Díaz, P., Fon-Sing, S., Fleury, G., and Sassi, J.-F. (2016). The Environmental
889 Biorefinery: Using Microalgae to Remediate Wastewater, a Win-Win Paradigm. *Energies* 9,
890 132. doi: 10.3390/en9030132.
- 891 Dincer, I., and Acar, C. (2015). Review and evaluation of hydrogen production methods for better
892 sustainability. *Int. J. Hydrogen Energy* 40, 11094–11111. doi: 10.1016/j.ijhydene.2014.12.035.
- 893 Donohoe, D. R., Collins, L. B., Wali, A., Bigler, R., Sun, W., and Bultman, S. J. (2012). The
894 Warburg Effect Dictates the Mechanism of Butyrate-Mediated Histone Acetylation and Cell

- 895 Proliferation. *Mol. Cell* 48, 612–626. doi: 10.1016/j.molcel.2012.08.033.
- 896 Duncan, S. H., Barcenilla, A., Stewart, C. S., Pryde, S. E., and Flint, H. J. (2002). Acetate Utilization
897 and Butyryl Coenzyme A (CoA):Acetate-CoA Transferase in Butyrate-Producing Bacteria from
898 the Human Large Intestine. *Appl. Environ. Microbiol.* 68, 5186–5190. doi:
899 10.1128/AEM.68.10.5186-5190.2002.
- 900 Durante, L., Hübner, W., Lauersen, K. J., and Remacle, C. (2019). Characterization of the
901 GPR1/FUN34/YaaH protein family in the green microalga *Chlamydomonas* suggests their role
902 as intracellular membrane acetate channels. *Plant Direct* 3. doi: 10.1002/pld3.148.
- 903 Fan, W., Gao, X. K., Rao, X. S., Shi, Y. P., Liu, X. C., Wang, F. Y., et al. (2018). Hsp70 Interacts
904 with Mitogen-Activated Protein Kinase (MAPK)-Activated Protein Kinase 2 To Regulate
905 p38MAPK Stability and Myoblast Differentiation during Skeletal Muscle Regeneration. *Mol.*
906 *Cell. Biol.* 38. doi: 10.1128/MCB.00211-18.
- 907 Faustino, R. S., Stronger, L. N. W., Richard, M. N., Czubyrt, M. P., Ford, D. A., Prociuk, M. A., et
908 al. (2007). RanGAP-Mediated Nuclear Protein Import in Vascular Smooth Muscle Cells Is
909 Augmented by Lysophosphatidylcholine. *Mol. Pharmacol.* 71, 438–445. doi:
910 10.1124/mol.105.021667.
- 911 Fei, Q., Fu, R., Shang, L., Brigham, C. J., and Chang, H. N. (2015). Lipid production by microalgae
912 *Chlorella protothecoides* with volatile fatty acids (VFAs) as carbon sources in heterotrophic
913 cultivation and its economic assessment. *Bioprocess Biosyst. Eng.* 38, 691–700. doi:
914 10.1007/s00449-014-1308-0.
- 915 Fleming, S. E., Fitch, M. D., DeVries, S., Liu, M. L., and Kight, C. (1991). Nutrient Utilization by
916 Cells Isolated from Rat Jejunum, Cecum and Colon. *J. Nutr.* 121, 869–878. doi:
917 10.1093/jn/121.6.869.
- 918 Fuentes-Ramírez, E. O., Vázquez-Acevedo, M., Cabrera-Orefice, A., Guerrero-Castillo, S., and
919 González-Halphen, D. (2021). The plastid proteome of the nonphotosynthetic chlorophycean
920 alga *Polytomella parva*. *Microbiol. Res.* 243. doi: 10.1016/j.micres.2020.126649.
- 921 Gabaldón, T. (2010). Peroxisome diversity and evolution. *Philos. Trans. R. Soc. B Biol. Sci.* 365,
922 765–773. doi: 10.1098/rstb.2009.0240.
- 923 Garrison, R. G., Mirikitani, F. K., Henry, D. P., Evans, B. J., and Arnold, W. N. (1985).
924 Ultrastructure of *Candida ingens*: a yeast that can assimilate volatile fatty acids. *Microbios* 42,
925 77–89.
- 926 Gerhardt, B. (1971). Zur Lokalisation von Enzymen der Microbodies in *Polytomella caeca*. *Arch.*
927 *Mikrobiol.* 80, 205–218. doi: 10.1007/BF00410122.
- 928 Gerhardt, B., and Berger, C. (1971). Microbodies und Diaminobenzidin-Reaktion in den Acetat-
929 Flagellaten *Polytomella caeca* und *Chlorogonium elongatum*. *Planta* 100, 155–166. Available
930 at: [http://sagdb.uni-](http://sagdb.uni-goettingen.de/showstrains.php?allfields=caeca&strain_number=&prev_name=&genus=&division=&species=&clas=&search= Show+strains1)
931 [goettingen.de/showstrains.php?allfields=caeca&strain_number=&prev_name=&genus=&divisio](http://sagdb.uni-goettingen.de/showstrains.php?allfields=caeca&strain_number=&prev_name=&genus=&division=&species=&clas=&search= Show+strains1)
932 [n=&species=&clas=&search= Show+strains1](http://sagdb.uni-goettingen.de/showstrains.php?allfields=caeca&strain_number=&prev_name=&genus=&division=&species=&clas=&search= Show+strains1).
- 933 Gonzalez, N. H., Felsner, G., Schramm, F. D., Klingl, A., Maier, U.-G., and Bolte, K. (2011). A
934 Single Peroxisomal Targeting Signal Mediates Matrix Protein Import in Diatoms. *PLoS One* 6,
935 e25316. doi: 10.1371/journal.pone.0025316.
- 936 Guan, X., Okazaki, Y., Zhang, R., Saito, K., and Nikolaua, B. J. (2020). Dual-localized enzymatic
937 components constitute the fatty acid synthase systems in mitochondria and plastids. *Plant*
938 *Physiol.* 183, 517–529. doi: 10.1104/pp.19.01564.
- 939 Haigh, W. G., and Beevers, H. (1964). The Glyoxylate cycle in *Polytomella caeca*. *Arch. Biochem.*
940 *Biophys.* 107, 152–157.
- 941 Harris, E. H. (1989). *The Chlamydomonas sourcebook*.
- 942 Harris, E. H. (2001). *Chlamydomonas* as a model organism. *Annu. Rev. Plant Physiol. Plant Mol.*
943 *Biol.* 52, 363–406. doi: 10.1146/annurev.arplant.52.1.363.

- 944 Hettema, E. H., van Roermund, C. W., Distel, B., van den Berg, M., Vilela, C., Rodrigues-Pousada,
945 C., et al. (1996). The ABC transporter proteins Pat1 and Pat2 are required for import of long-
946 chain fatty acids into peroxisomes of *Saccharomyces cerevisiae*. *EMBO J.* 15, 3813–22.
947 Available at: <http://www.ncbi.nlm.nih.gov/pubmed/8670886>.
- 948 Hosotani, K., Ohkochi, T., Inui, H., Yokota, A., Nakano, Y., and Kitaoka, S. (1988).
949 Photoassimilation of Fatty Acids, Fatty Alcohols and Sugars by *Euglena gracilis* Z.
950 *Microbiology* 134, 61–66. doi: 10.1099/00221287-134-1-61.
- 951 Hu, J., Baker, A., Bartel, B., Linka, N., Mullen, R. T., Reumann, S., et al. (2012). Plant Peroxisomes:
952 Biogenesis and Function. *Plant Cell* 24, 2279–2303. doi: 10.1105/tpc.112.096586.
- 953 Huerta-Cepas, J., Szklarczyk, D., Heller, D., Hernández-Plaza, A., Forslund, S. K., Cook, H., et al.
954 (2019). eggNOG 5.0: a hierarchical, functionally and phylogenetically annotated orthology
955 resource based on 5090 organisms and 2502 viruses. *Nucleic Acids Res.* 47, D309–D314. doi:
956 10.1093/nar/gky1085.
- 957 Hutner, S. H. (1972). Inorganic Nutrition. *Annu. Rev. Microbiol.* 26, 313–346. doi:
958 10.1146/annurev.mi.26.100172.001525.
- 959 Janssen, P. H., and Schink, B. (1995). Pathway of butyrate catabolism by *Desulfobacterium*
960 *cetonicum*. *J. Bacteriol.* 177, 3870–3872. doi: 10.1128/jb.177.13.3870-3872.1995.
- 961 Johnson, X., and Alric, J. (2013). Central carbon metabolism and electron transport in
962 *Chlamydomonas reinhardtii*: Metabolic constraints for carbon partitioning between oil and
963 starch. *Eukaryot. Cell* 12, 776–793. doi: 10.1128/EC.00318-12.
- 964 Karnaouri, A., Chalima, A., Kalogiannis, K. G., Varamogianni-Mamatsi, D., Lappas, A., and
965 Topakas, E. (2020). Utilization of lignocellulosic biomass towards the production of omega-3
966 fatty acids by the heterotrophic marine microalga *Cryptocodinium cohnii*. *Bioresour. Technol.*
967 303, 122899. doi: 10.1016/j.biortech.2020.122899.
- 968 Kato, N., Nelson, G., and Lauersen, K. J. (2021). Subcellular Localizations of Catalase and
969 Exogenously Added Fatty Acid in *Chlamydomonas reinhardtii*. *Cells* 10, 1940. Available at:
970 <https://www.mdpi.com/2073-4409/10/8/1940>.
- 971 Kong, F., Liang, Y., Légeret, B., Beyly-Adriano, A., Blangy, S., Haslam, R. P., et al. (2017).
972 *Chlamydomonas* carries out fatty acid β -oxidation in ancestral peroxisomes using a bona fide
973 acyl-CoA oxidase. *Plant J.* 90, 358–371. doi: 10.1111/tpj.13498.
- 974 Krieger-Liszkay, A., and Feilke, K. (2016). The Dual Role of the Plastid Terminal Oxidase PTOX:
975 Between a Protective and a Pro-oxidant Function. *Front. Plant Sci.* 6. doi:
976 10.3389/fpls.2015.01147.
- 977 Kunze, M., Pracharoenwattana, I., Smith, S. M., and Hartig, A. (2006). A central role for the
978 peroxisomal membrane in glyoxylate cycle function. *Biochim. Biophys. Acta - Mol. Cell Res.*
979 1763, 1441–1452. doi: 10.1016/j.bbamcr.2006.09.009.
- 980 Lacroux, J., Seira, J., Trably, E., Bernet, N., Steyer, J., and van Lis, R. (2021). Mixotrophic Growth
981 of *Chlorella sorokiniana* on Acetate and Butyrate : Interplay Between Substrate , C : N Ratio and
982 pH. *Front. Microbiol.* 12, 1–16. doi: 10.3389/fmicb.2021.703614.
- 983 Lacroux, J., Trably, E., Bernet, N., Steyer, J. P., and van Lis, R. (2020). Mixotrophic growth of
984 microalgae on volatile fatty acids is determined by their undissociated form. *Algal Res.* 47,
985 101870. doi: 10.1016/j.algal.2020.101870.
- 986 Lauersen, K. J., Willamme, R., Coosemans, N., Joris, M., Kruse, O., and Remacle, C. (2016).
987 Peroxisomal microbodies are at the crossroads of acetate assimilation in the green microalga
988 *Chlamydomonas reinhardtii*. *Algal Res.* 16, 266–274. doi: 10.1016/j.algal.2016.03.026.
- 989 Li-Beisson, Y., Beisson, F., and Riekhof, W. (2015). Metabolism of acyl-lipids in *Chlamydomonas*
990 *reinhardtii*. *Plant J.* 82, 504–522. doi: 10.1111/tpj.12787.
- 991 Li-Beisson, Y., Shorosh, B., Beisson, F., Andersson, M. X., Arondel, V., Bates, P. D., et al. (2013).
992 Acyl-Lipid Metabolism. *Arab. B.* 11, e0161. doi: 10.1199/tab.0161.

- 993 Li-Beisson, Y., Thelen, J. J., Fedosejevs, E., and Harwood, J. L. (2019). The lipid biochemistry of
994 eukaryotic algae. *Prog. Lipid Res.* 74, 31–68. doi: 10.1016/j.plipres.2019.01.003.
- 995 Liang, Y., Kong, F., Torres-Romero, I., Burlacot, A., Cuine, S., Légeret, B., et al. (2019). Branched-
996 Chain Amino Acid Catabolism Impacts Triacylglycerol Homeostasis in *Chlamydomonas*
997 *reinhardtii*. *Plant Physiol.* 179, 1502–1514. doi: 10.1104/pp.18.01584.
- 998 Liebthal, M., Maynard, D., and Dietz, K.-J. (2018). Peroxiredoxins and Redox Signaling in Plants.
999 *Antioxid. Redox Signal.* 28, 609–624. doi: 10.1089/ars.2017.7164.
- 1000 Linka, N., and Theodoulou, F. L. (2013). “Metabolite Transporters of the Plant Peroxisomal
1001 Membrane: Known and Unknown,” in, 169–194. doi: 10.1007/978-94-007-6889-5_10.
- 1002 Liu, C. H., Chang, C. Y., Liao, Q., Zhu, X., and Chang, J. S. (2013). Photoheterotrophic growth of
1003 *Chlorella vulgaris* ESP6 on organic acids from dark hydrogen fermentation effluents. *Bioresour.*
1004 *Technol.* 145, 331–336. doi: 10.1016/j.biortech.2012.12.111.
- 1005 Llamas, M., Dourou, M., González-Fernández, C., Aggelis, G., and Tomás-Pejó, E. (2020).
1006 Screening of oleaginous yeasts for lipid production using volatile fatty acids as substrate.
1007 *Biomass and Bioenergy* 138, 1–10. doi: 10.1016/j.biombioe.2020.105553.
- 1008 Lloyd, D., Evans, D. A., and Venables, S. E. (1968). Propionate assimilation in the flagellate
1009 *Polytomella caeca*. An inducible mitochondrial enzyme system. *Biochem. J.* 109, 897–907. doi:
1010 10.1042/bj1090897.
- 1011 Lu, W., Du, J., Schwarzer, N. J., Gerbig-Smentek, E., Einsle, O., and Andrade, S. L. A. (2012). The
1012 formate channel FocA exports the products of mixed-acid fermentation. *Proc. Natl. Acad. Sci.*
1013 109, 13254–13259. doi: 10.1073/pnas.1204201109.
- 1014 May, P., Wienkoop, S., Kempa, S., Usadel, B., Christian, N., Rupprecht, J., et al. (2008).
1015 Metabolomics- and Proteomics-Assisted Genome Annotation and Analysis of the Draft
1016 Metabolic Network of *Chlamydomonas reinhardtii*. *Genetics* 179, 157–166. doi:
1017 10.1534/genetics.108.088336.
- 1018 McCommis, K. S., and Finck, B. N. (2015). Mitochondrial pyruvate transport: a historical
1019 perspective and future research directions. *Biochem. J.* 466, 443–454. doi: 10.1042/BJ20141171.
- 1020 Mentzen, W. I., Peng, J., Ransom, N., Nikolau, B. J., and Wurtele, E. S. (2008). Articulation of three
1021 core metabolic processes in *Arabidopsis*: Fatty acid biosynthesis, leucine catabolism and starch
1022 metabolism. *BMC Plant Biol.* 8, 76. doi: 10.1186/1471-2229-8-76.
- 1023 Millar, A. H., and Heazlewood, J. L. (2003). Genomic and Proteomic Analysis of Mitochondrial
1024 Carrier Proteins in *Arabidopsis*. *Plant Physiol.* 131, 443–453. doi: 10.1104/pp.009985.
- 1025 Mishra, S. K., Suh, W. I., Farooq, W., Moon, M., Shrivastav, A., Park, M. S., et al. (2014). Rapid
1026 quantification of microalgal lipids in aqueous medium by a simple colorimetric method.
1027 *Bioresour. Technol.* 155, 330–333. doi: 10.1016/j.biortech.2013.12.077.
- 1028 Morth, J. P., Pedersen, B. P., Buch-Pedersen, M. J., Andersen, J. P., Vilsen, B., Palmgren, M. G., et
1029 al. (2011). A structural overview of the plasma membrane Na⁺,K⁺-ATPase and H⁺-ATPase ion
1030 pumps. *Nat. Rev. Mol. Cell Biol.* 12, 60–70. doi: 10.1038/nrm3031.
- 1031 Moscoviz, R., Trably, E., Bernet, N., and Carrère, H. (2018). The environmental biorefinery: State-
1032 of-the-art on the production of hydrogen and value-added biomolecules in mixed-culture
1033 fermentation. *Green Chem.* 20, 3159–3179. doi: 10.1039/c8gc00572a.
- 1034 Neilson, A. H., and Lewin, R. A. (1974). The uptake and utilization of organic carbon by algae: an
1035 essay in comparative biochemistry. *Phycologia* 13, 227–264. doi: 10.2216/i0031-8884-13-3-
1036 227.1.
- 1037 Nogaj, L. A., Srivastava, A., van Lis, R., and Beale, S. I. (2005). Cellular levels of glutamyl-tRNA
1038 reductase and glutamate-1-semialdehyde aminotransferase do not control chlorophyll synthesis
1039 in *Chlamydomonas reinhardtii*. *Plant Physiol.* 139, 389–396. doi: 10.1104/pp.105.067009.
- 1040 Nolte, J. C., Schürmann, M., Schepers, C. L., Vogel, E., Wübbeler, J. H., and Steinbüchel, A. (2014).
1041 Novel characteristics of succinate coenzyme a (succinate-coa) ligases: Conversion of malate to

- 1042 malyl-coa and coa-thioester formation of succinate analogues in vitro. *Appl. Environ. Microbiol.*
1043 80, 166–176. doi: 10.1128/AEM.03075-13.
- 1044 Ouyang, Y., Chen, J., Xie, W., Wang, L., and Zhang, Q. (2009). Comprehensive sequence and
1045 expression profile analysis of Hsp20 gene family in rice. *Plant Mol. Biol.* 70, 341–357. doi:
1046 10.1007/s11103-009-9477-y.
- 1047 Ouyang, Y., Wu, Q., Li, J., Sun, S., and Sun, S. (2020). S-adenosylmethionine: A metabolite critical
1048 to the regulation of autophagy. *Cell Prolif.* 53. doi: 10.1111/cpr.12891.
- 1049 Pan, R., Liu, J., Wang, S., and Hu, J. (2020). Peroxisomes: versatile organelles with diverse roles in
1050 plants. *New Phytol.* 225, 1410–1427. doi: 10.1111/nph.16134.
- 1051 Pan, Y., Yang, J., Gong, Y., Li, X., and Hu, H. (2017). 3-Hydroxyisobutyryl-CoA hydrolase involved
1052 in isoleucine catabolism regulates triacylglycerol accumulation in *Phaeodactylum tricoratum*.
1053 *Philos. Trans. R. Soc. B Biol. Sci.* 372, 20160409. doi: 10.1098/rstb.2016.0409.
- 1054 Perez-Garcia, O., and Bashan, Y. (2015). “Microalgal Heterotrophic and Mixotrophic Culturing for
1055 Bio-refining: From Metabolic Routes to Techno-economics,” in *Algal Biorefineries* (Cham:
1056 Springer International Publishing), 61–131. doi: 10.1007/978-3-319-20200-6_3.
- 1057 Perez-Garcia, O., Escalante, F. M. E., de-Bashan, L. E., and Bashan, Y. (2011). Heterotrophic
1058 cultures of microalgae: Metabolism and potential products. *Water Res.* 45, 11–36. doi:
1059 10.1016/J.WATRES.2010.08.037.
- 1060 Perez-Riverol, Y., Bai, J., Bandla, C., García-Seisdedos, D., Hewapathirana, S., Kamatchinathan, S.,
1061 et al. (2022). The PRIDE database resources in 2022: a hub for mass spectrometry-based
1062 proteomics evidences. *Nucleic Acids Res.* 50, D543–D552. doi: 10.1093/nar/gkab1038.
- 1063 Petrova, V. Y., Drescher, D., Kujumdzieva, A. V., and Schmitt, M. J. (2004). Dual targeting of yeast
1064 catalase A to peroxisomes and mitochondria. *Biochem. J.* 380, 393–400. doi:
1065 10.1042/bj20040042.
- 1066 Pietrocola, F., Galluzzi, L., Bravo-San Pedro, J. M., Madeo, F., and Kroemer, G. (2015). Acetyl
1067 coenzyme A: a central metabolite and second messenger. *Cell Metab.* 21, 805–821. doi:
1068 10.1016/j.cmet.2015.05.014.
- 1069 Rezayian, M., Niknam, V., and Ebrahimzadeh, H. (2019). Oxidative damage and antioxidative
1070 system in algae. *Toxicol. Reports* 6, 1309–1313. doi: 10.1016/j.toxrep.2019.10.001.
- 1071 Riekhof, W. R., Sears, B. B., and Benning, C. (2005). Annotation of genes involved in glycerolipid
1072 biosynthesis in *Chlamydomonas reinhardtii*: Discovery of the betaine lipid synthase BTA1Cr.
1073 *Eukaryot. Cell* 4, 242–252. doi: 10.1128/EC.4.2.242-252.2005.
- 1074 Roediger, W. E. (1982). Utilization of nutrients by isolated epithelial cells of the rat colon.
1075 *Gastroenterology* 83, 424–429.
- 1076 Rottensteiner, H., and Theodoulou, F. L. (2006). The ins and outs of peroxisomes: Co-ordination of
1077 membrane transport and peroxisomal metabolism. *Biochim. Biophys. Acta - Mol. Cell Res.*
1078 1763, 1527–1540. doi: 10.1016/j.bbamcr.2006.08.012.
- 1079 Round, F. (1980). The evolution of pigmented and unpigmented unicells - a reconsideration of the
1080 Protista. *BioSystems* 12, 61–69.
- 1081 Roy, U. K., Nielsen, B. V., and Milledge, J. J. (2021). Antioxidant production in *Dunaliella*. *Appl.*
1082 *Sci.* 11, 1–24. doi: 10.3390/app11093959.
- 1083 Schwacke, R., Ponce-Soto, G. Y., Krause, K., Bolger, A. M., Arsova, B., Hallab, A., et al. (2019).
1084 MapMan4: A Refined Protein Classification and Annotation Framework Applicable to Multi-
1085 Omics Data Analysis. *Mol. Plant* 12, 879–892. doi: 10.1016/j.molp.2019.01.003.
- 1086 Schwanhäusser, B., Busse, D., Li, N., Dittmar, G., Schuchhardt, J., Wolf, J., et al. (2011). Global
1087 quantification of mammalian gene expression control. *Nature* 473, 337–342. doi:
1088 10.1038/nature10098.
- 1089 Sheeler, P., Moore, J., Cantor, M., and Granik, R. (1968). The stored polysaccharide of *Polytomella*
1090 *agilis*. *Life Sci.* 7, 1045–1051. doi: 10.1016/0024-3205(68)90141-0.

- 1091 Shtaida, N., Khozin-Goldberg, I., and Boussiba, S. (2015). The role of pyruvate hub enzymes in
1092 supplying carbon precursors for fatty acid synthesis in photosynthetic microalgae. *Photosynth.*
1093 *Res.* 125, 407–422. doi: 10.1007/s11120-015-0136-7.
- 1094 Silverberg, B. A. (1975). An ultrastructural and cytochemical characterization of microbodies in the
1095 green algae. *Protoplasma* 83, 269–295. doi: 10.1007/BF01282559.
- 1096 Smith, D. R., and Lee, R. W. (2014). A plastid without a genome: evidence from the
1097 nonphotosynthetic green algal genus *Polytomella*. *Plant Physiol.* 164, 1812–1819. doi:
1098 10.1104/pp.113.233718.
- 1099 Soares-Silva, M., Diniz, F. F., Gomes, G. N., and Bahia, D. (2016). The Mitogen-Activated Protein
1100 Kinase (MAPK) Pathway: Role in Immune Evasion by Trypanosomatids. *Front. Microbiol.* 7.
1101 doi: 10.3389/fmicb.2016.00183.
- 1102 Sousa, R. H. V., Carvalho, F. E. L., Lima-Melo, Y., Alencar, V. T. C. B., Daloso, D. M., Margis-
1103 Pinheiro, M., et al. (2019). Impairment of peroxisomal APX and CAT activities increases
1104 protection of photosynthesis under oxidative stress. *J. Exp. Bot.* 70, 627–639. doi:
1105 10.1093/jxb/ery354.
- 1106 Strauch, A., and Haslbeck, M. (2016). The function of small heat-shock proteins and their
1107 implication in proteostasis. *Essays Biochem.* 60, 163–172. doi: 10.1042/EBC20160010.
- 1108 Tardif, M., Atteia, A., Specht, M., Cogne, G., Rolland, N., Brugière, S., et al. (2012). PredAlgo: A
1109 New Subcellular Localization Prediction Tool Dedicated to Green Algae. *Mol. Biol. Evol.* 29,
1110 3625–3639. doi: 10.1093/molbev/mss178.
- 1111 Turon, V., Baroukh, C., Trably, E., Latrille, E., Fouilland, E., and Steyer, J.-P. (2015). Use of
1112 fermentative metabolites for heterotrophic microalgae growth: Yields and kinetics. *Bioresour.*
1113 *Technol.* 175, 342–349. doi: 10.1016/J.BIORTECH.2014.10.114.
- 1114 Turon, V., Trably, E., Fouilland, E., and Steyer, J.-P. (2016). Potentialities of dark fermentation
1115 effluents as substrates for microalgae growth: A review. *Process Biochem.* 51, 1843–1854. doi:
1116 10.1016/J.PROCBIO.2016.03.018.
- 1117 van Lis, R., and Atteia, A. (2004). Control of Mitochondrial Function via Photosynthetic Redox
1118 Signals. *Photosynth. Res.* 79, 133–148. doi: 10.1023/B:PRES.0000015409.14871.68.
- 1119 van Lis, R., Couté, Y., Brugière, S., Tourasse, N. J., Laurent, B., Nitschke, W., et al. (2021).
1120 Phylogenetic and functional diversity of aldehyde-alcohol dehydrogenases in microalgae. *Plant*
1121 *Mol. Biol.* 105, 497–511. doi: 10.1007/s11103-020-01105-9.
- 1122 van Roermund, C. W. T., Schroers, M. G., Wiese, J., Facchinelli, F., Kurz, S., Wilkinson, S., et al.
1123 (2016). The Peroxisomal NAD Carrier from *Arabidopsis* Imports NAD in Exchange with AMP.
1124 *Plant Physiol.* 171, 2127–2139. doi: 10.1104/pp.16.00540.
- 1125 van Roermund, C. W. T., Tabak, H. F., van den Berg, M., Wanders, R. J. A., and Hettema, E. H.
1126 (2000). Pex11p Plays a Primary Role in Medium-Chain Fatty Acid Oxidation, a Process That
1127 Affects Peroxisome Number and Size in *Saccharomyces cerevisiae*. *J. Cell Biol.* 150, 489–498.
1128 doi: 10.1083/jcb.150.3.489.
- 1129 Walter, K. A., Nair, R. V., Cary, J. W., Bennett, G. N., and Papoutsakis, E. T. (1993). Sequence and
1130 arrangement of two genes of the butyrate-synthesis pathway of *Clostridium acetobutylicum*
1131 ATCC 824. *Gene* 134, 107–111. doi: 10.1016/0378-1119(93)90182-3.
- 1132 Wieczorek, S., Combes, F., Lazar, C., Gai Gianetto, Q., Gatto, L., Dorffer, A., et al. (2017). DAPAR
1133 & ProStaR: software to perform statistical analyses in quantitative discovery proteomics.
1134 *Bioinformatics* 33, 135–136. doi: 10.1093/bioinformatics/btw580.
- 1135 Wise, D. L. (1955). Carbon Sources for *Polytomella caeca*. *J. Protozool.* 2, 156–158. doi:
1136 10.1111/j.1550-7408.1955.tb02416.x.
- 1137 Wise, D. L. (1959). Carbon Nutrition and Metabolism of *Polytomella caeca*. *J. Protozool.* 6, 19–23.
1138 doi: 10.1111/j.1550-7408.1959.tb03921.x.
- 1139 Wise, D. L. (1968). Effects of Acetaldehyde on Growth and Biosynthesis in an Algal Flagellate

- 1140 Polytomella caeca. *J. Protozool.* 15, 528–531. doi: 10.1111/j.1550-7408.1968.tb02169.x.
1141 Wu, T., Fu, Y., Shi, Y., Li, Y., Kou, Y., Mao, X., et al. (2020). Functional Characterization of Long-
1142 Chain Acyl-CoA Synthetase Gene Family from the Oleaginous Alga *Chromochloris*
1143 *zofingiensis*. *J. Agric. Food Chem.* 68, 4473–4484. doi: 10.1021/acs.jafc.0c01284.
1144 Xu, X., Zhang, L., Zhao, W., Fu, L., Han, Y., Wang, K., et al. (2021). Genome-wide analysis of the
1145 serine carboxypeptidase-like protein family in *Triticum aestivum* reveals TaSCPL184-6D is
1146 involved in abiotic stress response. *BMC Genomics* 22, 350. doi: 10.1186/s12864-021-07647-6.
1147 Yemm, E. W., and Willis, A. J. (1954). The estimation of carbohydrates in plant extracts by anthrone.
1148 *Biochem. J.* 57, 508–14. Available at: <http://www.ncbi.nlm.nih.gov/pubmed/13181867>.
1149 Zhan, J., Rong, J., and Wang, Q. (2017). Mixotrophic cultivation, a preferable microalgae cultivation
1150 mode for biomass/bioenergy production, and bioremediation, advances and prospect. *Int. J.*
1151 *Hydrogen Energy* 42, 8505–8517. doi: 10.1016/j.ijhydene.2016.12.021.
1152

1153 **10 Supplementary Material**

- 1154 Supplementary Table I. Differential analysis of total proteomes from *Polytomella* sp. grown on
1155 acetate or butyrate.

1156 **11 Data Availability Statement**

- 1157 The mass spectrometry proteomics data have been deposited to the ProteomeXchange Consortium
1158 via the PRIDE partner repository with the dataset identifier PXD035155
1159 (<https://www.ebi.ac.uk/pride/login>)

1160

1161 **12 Figures**

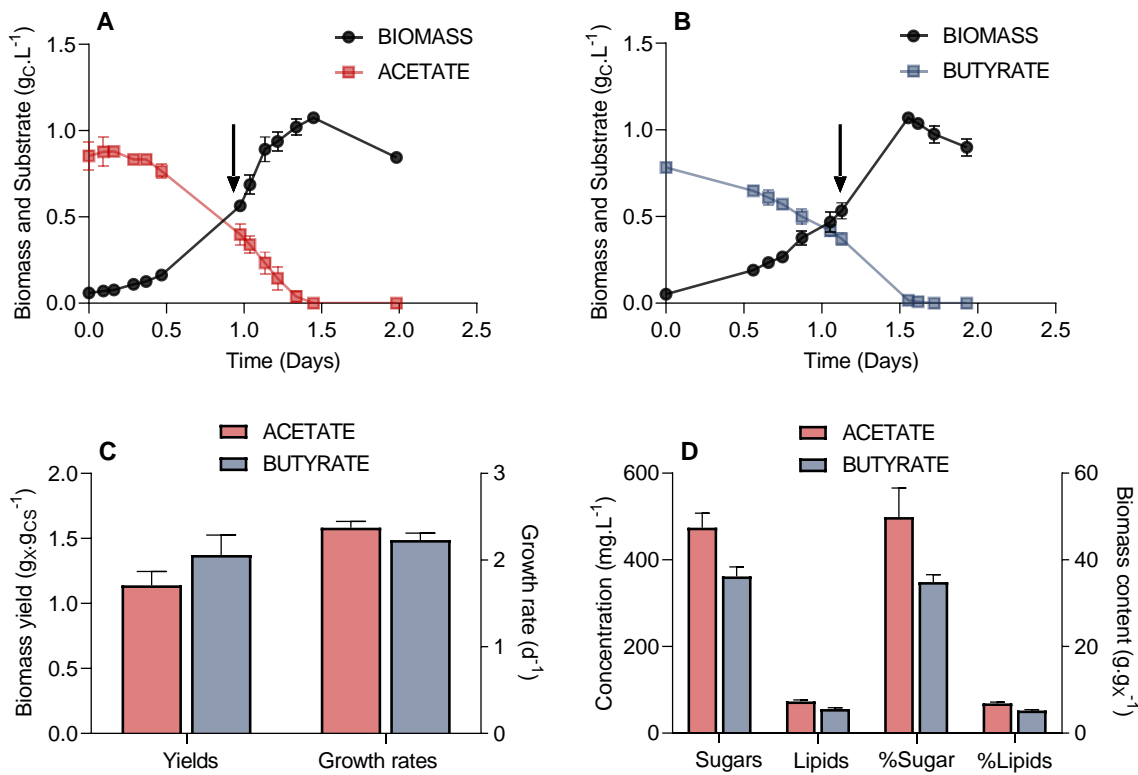


Figure 1. Parameters of the growth of *Polytomella* sp. on acetate and butyrate. A,B) Growth curves ($g_X \cdot L^{-1}$) and substrate consumption ($g_{CS} \cdot L^{-1}$) of *Polytomella* sp. in presence of $1 g_{CS} \cdot L^{-1}$ acetate or butyrate, C) biomass yields ($g_X \cdot g_{CS}^{-1}$) and growth rates (d^{-1}) derived from these growth curves and D) the concentrations of sugars and lipids are plotted on the left ($g \cdot L^{-1}$) while their proportions to the total biomass are plotted on the right ($g \cdot g_X^{-1}$) for both conditions. Arrows indicate when biomass for further proteomics analysis was sampled. X, dry weight; CS, dissolved organic carbon. Error bars correspond to standard deviations based on 3 biological replicates.

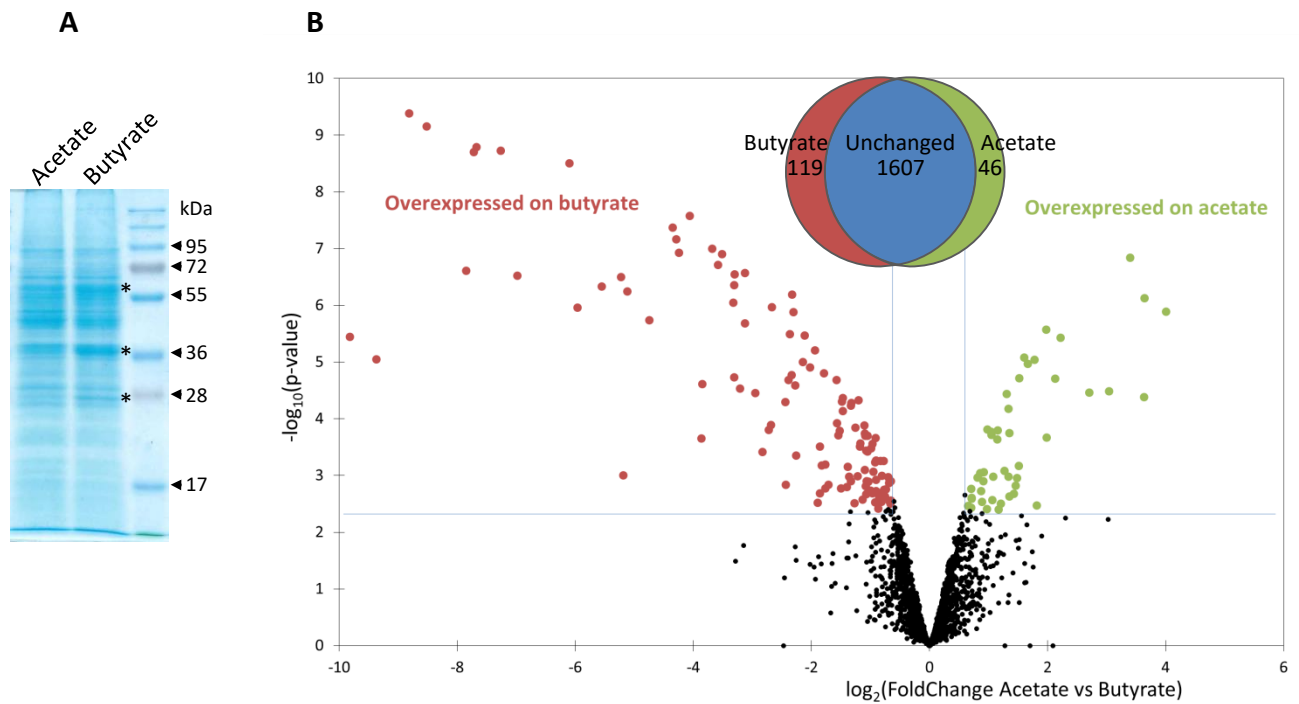
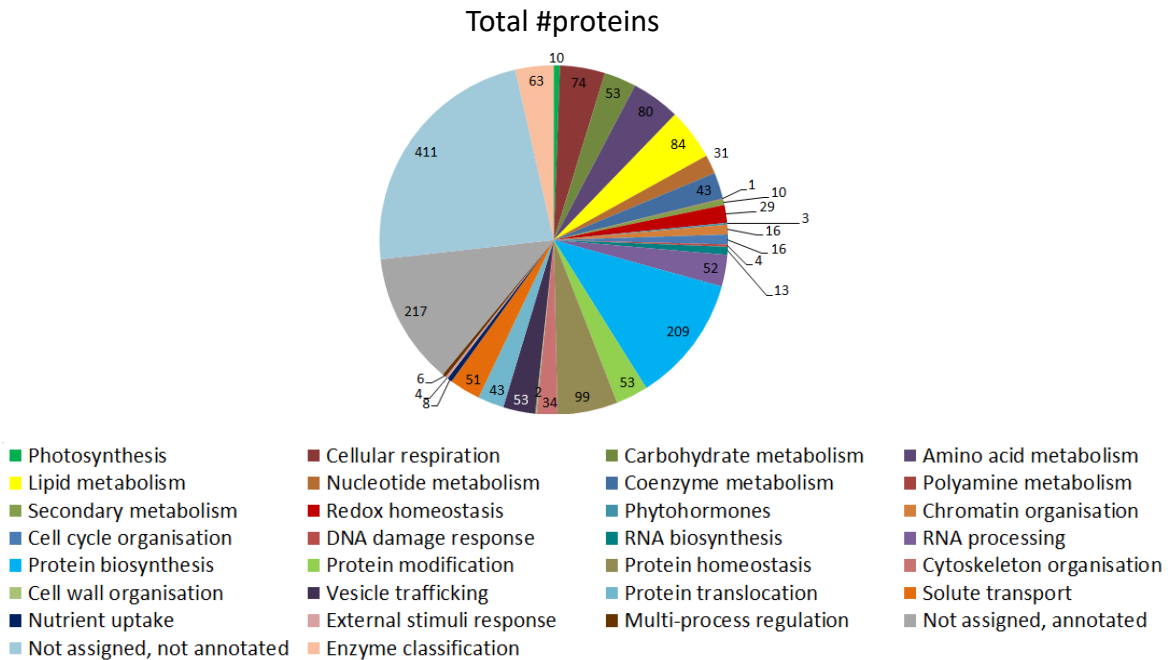


Figure 2. Comparison of global proteomes of *Polytomella* sp. grown on acetate and butyrate. A) Total proteins (30 μg) of *Polytomella* sp. growing exponentially on acetate or butyrate, resolved in a 12% SDS-polyacrylamide gel stained with Coomassie Blue G250. B) Volcano plot displaying the differential abundance of proteins of *Polytomella* sp. grown on acetate or butyrate analysed by MS-based quantitative proteomics. The volcano plot represents the $-\log_{10}(\text{limma } p\text{-value})$, cut off 0.004 on y-axis plotted against the $\log_2(\text{FoldChange acetate/butyrate})$ on the x-axis. Green and red dots represent proteins found more abundant in *Polytomella* sp. grown respectively on acetate or butyrate (Benjamini-Hochberg FDR < 1%). The Venn diagram indicates that of the total of 1772 proteins detected for acetate and butyrate combined, 48 were significantly induced on acetate and 117 on butyrate.a

A)



B)

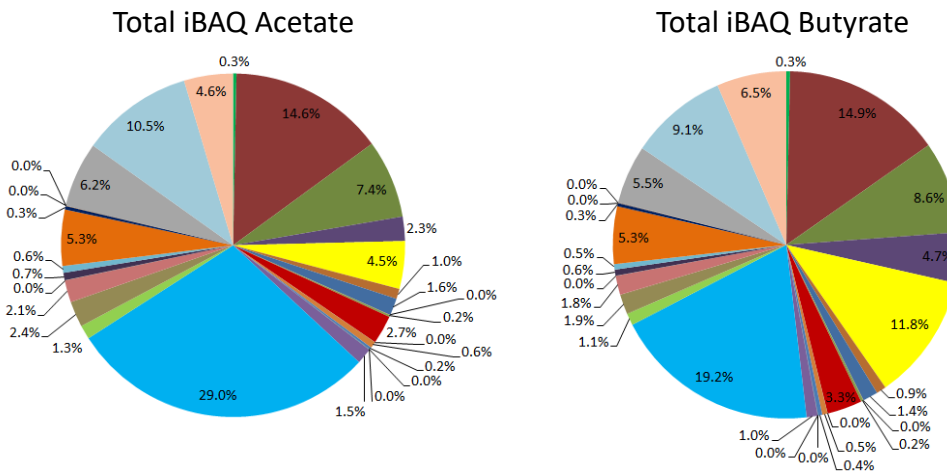


Figure 3. Overview of the *Polytomella* proteome revealed by the differential approach, represented per metabolic category as determined by Mercator. A) Total number of proteins identified in both acetate and butyrate-growing cells. B) Cumulative iBAQ values of total acetate and butyrate proteomes give an indication of the total protein abundance per category.

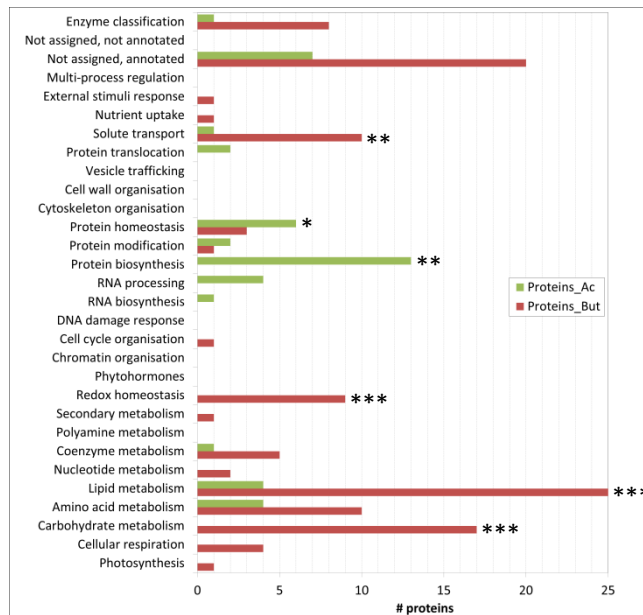


Figure 4. Focus on differentially expressed proteins, *i.e.* with a statistically significant difference in FC value. The number of proteins per category is given that are significantly more induced on either acetate or butyrate. Categories with a significant difference in FC proteins between either the acetate or the butyrate condition with respect to the background in the Fisher test are indicated with one asterisk (p -value <0.05), two asterisks (p <0.01) or three asterisks (p <0.001). Note that some categories do not contain any differentially expressed proteins, and the fact that some categories do not exhibit any FC proteins in either the acetate or butyrate condition does not mean there is no protein.

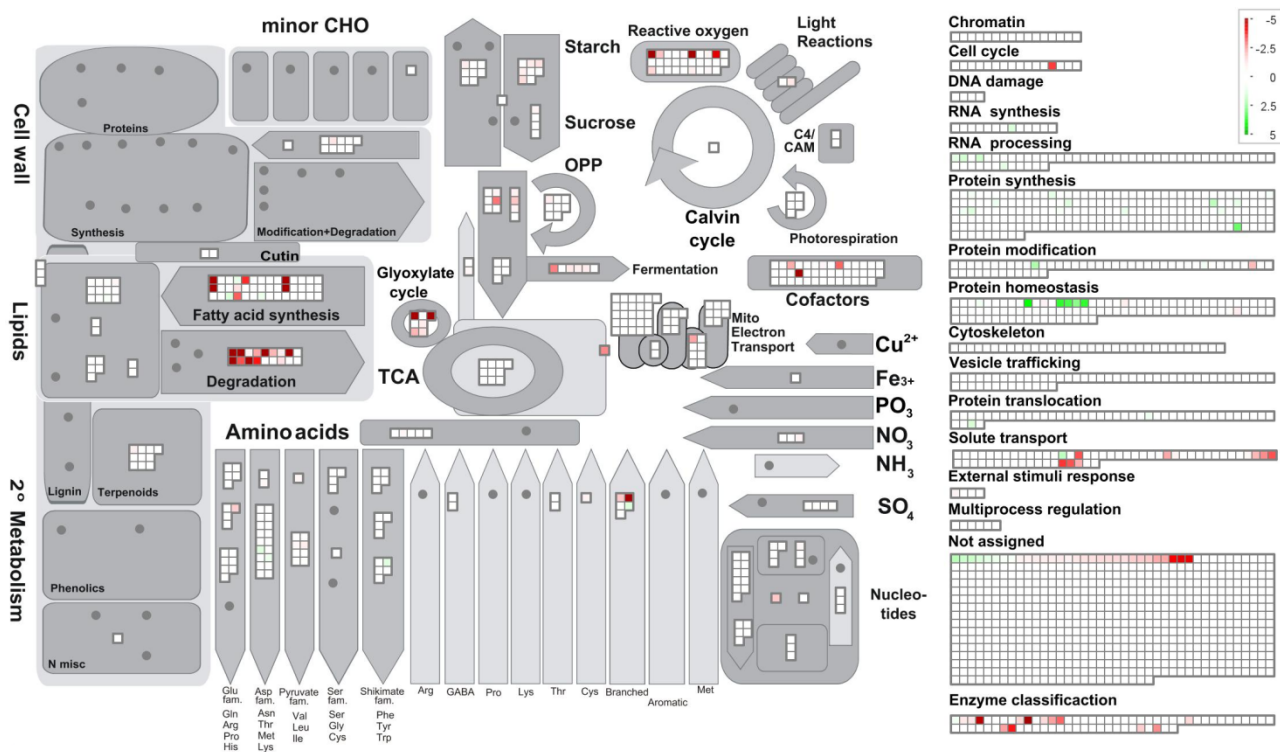


Figure 5. Schematic representation of cellular metabolism as a function of metabolic (sub)categories and log₂ FoldChange values using the program MapMan. Metabolic categories were analyzed using the web program Mercator. For all entries with a FC score applies p-value <0.004. Note that for increased visibility of the lower range of the log₂ FC scale was set from 5 to -5 whereas a few proteins on butyrate actually show higher FC values.

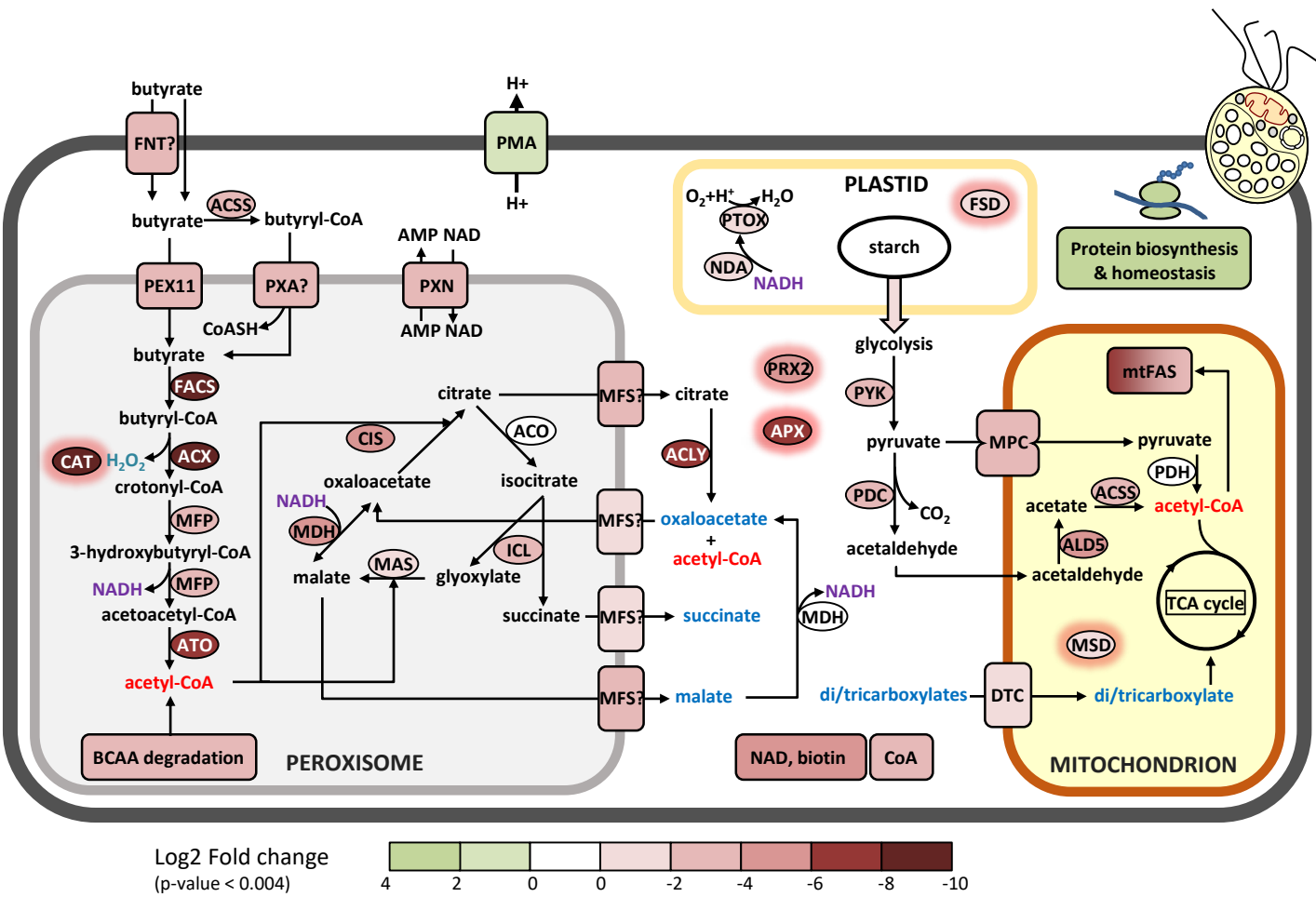


Figure 6. Proposed metabolic reconstruction of the assimilation pathway of butyrate in the peroxisome and interactions with other cell compartments. Taken into account are the FoldChange values and cellular localization based on software prediction (DeepLoc), manual verification of targeting signals and previous studies. The log₂ FC acetate/butyrate value is indicated by the color codes. All di/tricarboxylic acids that may be imported into the mitochondria are indicated in blue. Enzymes with a red halo are involved in antioxidant defense. Enzymes codes and further information can be found in Table I and the Suppl. Table.

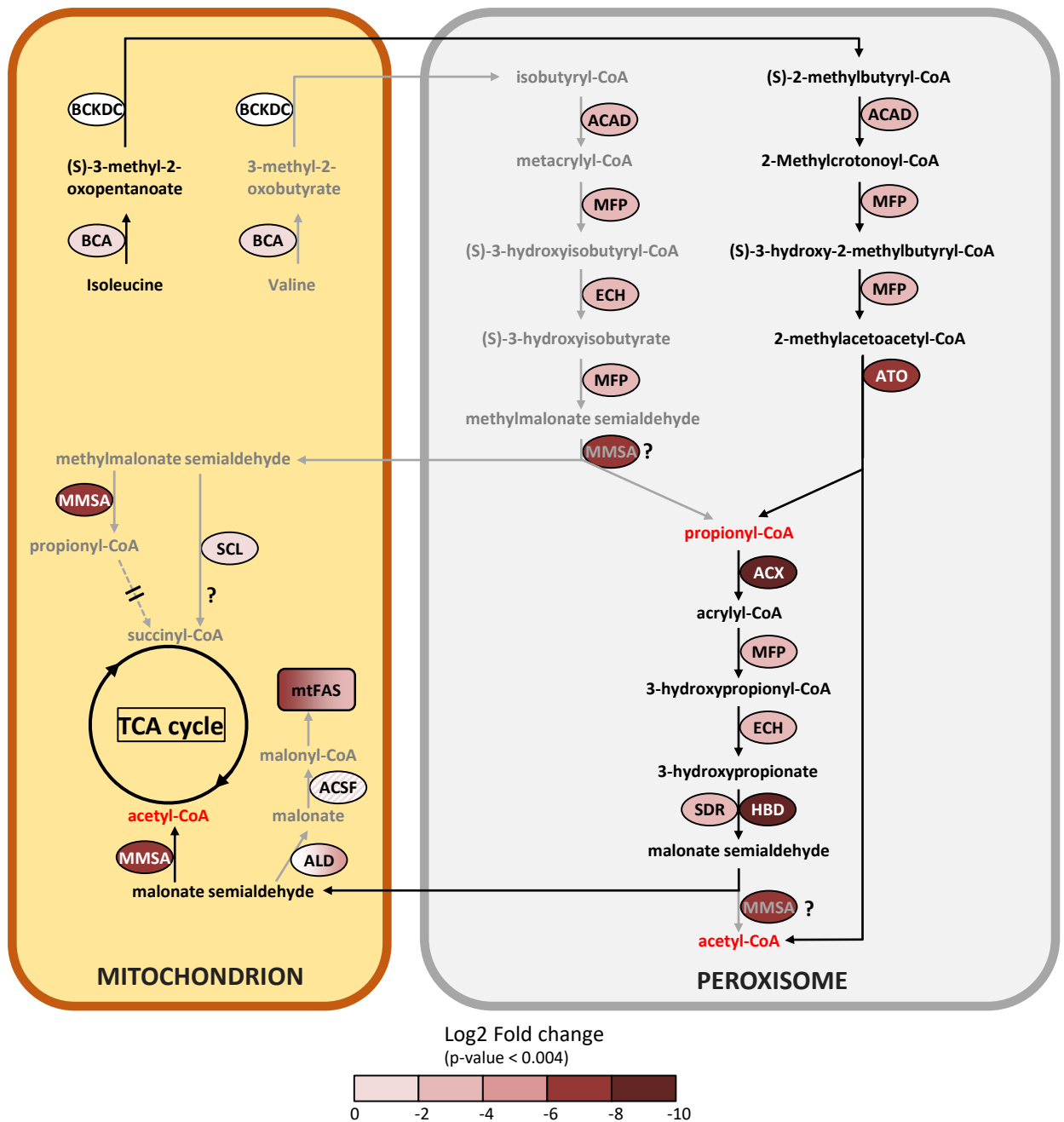


Figure 7. Metabolic reconstruction of the branched amino acid degradation pathway in the peroxisome and proposed interactions with the mitochondria. The log₂ fold change But/Ac is indicated by the color codes. Further information can be found in Table I. Arrows in grey represent less likely or hypothetical pathways, proposed pathways use black arrows. ACSF exhibits an FC value with p>0.004. ALD color gradient indicates different isoforms with FC values between 0-6.